

12-2016

Assessing the Potential Clinical Impact of Variable Biological Effectiveness in Proton Radiotherapy

Christopher R. Peeler Ph.D.

Follow this and additional works at: https://digitalcommons.library.tmc.edu/utgsbs_dissertations



Part of the [Medical Biomathematics and Biometrics Commons](#), and the [Other Physics Commons](#)

Recommended Citation

Peeler, Christopher R. Ph.D., "Assessing the Potential Clinical Impact of Variable Biological Effectiveness in Proton Radiotherapy" (2016). *The University of Texas MD Anderson Cancer Center UTHealth Graduate School of Biomedical Sciences Dissertations and Theses (Open Access)*. 709.
https://digitalcommons.library.tmc.edu/utgsbs_dissertations/709

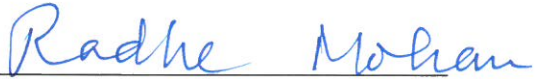
This Dissertation (PhD) is brought to you for free and open access by the The University of Texas MD Anderson Cancer Center UTHealth Graduate School of Biomedical Sciences at DigitalCommons@TMC. It has been accepted for inclusion in The University of Texas MD Anderson Cancer Center UTHealth Graduate School of Biomedical Sciences Dissertations and Theses (Open Access) by an authorized administrator of DigitalCommons@TMC. For more information, please contact digitalcommons@library.tmc.edu.

ASSESSING THE POTENTIAL CLINICAL IMPACT OF VARIABLE BIOLOGICAL
EFFECTIVENESS IN PROTON RADIOTHERAPY

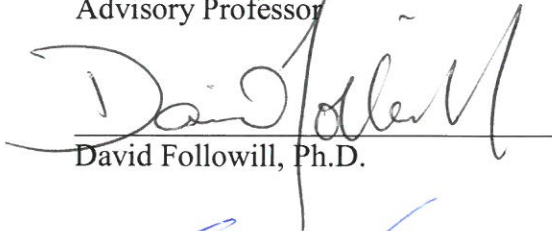
by

Christopher Ryan Peeler, B.S.

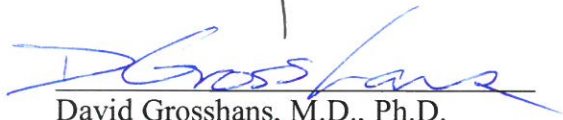
APPROVED:




Radhe Mohan, Ph.D.
Advisory Professor



David Followill, Ph.D.



David Grosshans, M.D., Ph.D.



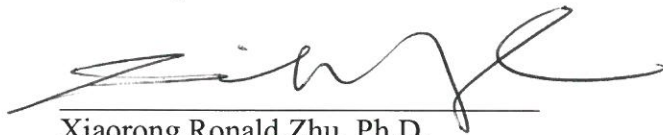
Dragan Mirkovic, Ph.D.



Arvind Rao, Ph.D.



Uwe Titt, Ph.D.



Xiaorong Ronald Zhu, Ph.D.

APPROVED:

Dean, The University of Texas
Graduate School of Biomedical Sciences at Houston

ASSESSING THE POTENTIAL CLINICAL IMPACT OF VARIABLE BIOLOGICAL
EFFECTIVENESS IN PROTON RADIOTHERAPY

A

DISSERTATION

Presented to the Faculty of
The University of Texas
Health Science Center at Houston
and
The University of Texas
MD Anderson Cancer Center
Graduate School of Biomedical Sciences
in Partial Fulfillment

of the Requirements

for the Degree of

DOCTOR OF PHILOSOPHY

by

Christopher Ryan Peeler, B.S.
Houston, Texas

December, 2016

DEDICATION

This work is dedicated to my family, both immediate and extended.

Thank you for your unending love and support!

Acknowledgements

Pursuing a Ph.D. is not something many people do, and it is not certainly not something many people from South Louisiana do. I am forever grateful to my family, immediate and extended, for continually encouraging me to pursue my interests and to strive to achieve as much as I possibly could. When I doubted myself and questioned whether or not what I was pursuing was worth it, I was reminded that I was loved unconditionally and that it didn't matter what path I took as long as I was happy. This gave me strength to push on, and I would not be where I am today were it not for the unwavering support they have provided for me.

Throughout my graduate career, I have had the pleasure and privilege of learning from many outstanding mentors who have invested their time and effort into ensuring my success. I am indebted to my advisor Dr. Radhe Mohan for the training he has provided through my six years of graduate school. As a result of his training, I have learned to approach problems from the perspective of translation – always having the goal of identifying problems whose solutions will directly improve the lives of the patients we treat. I have also learned to approach problems with application in mind, even when the science at hand is basic in nature. Beyond research, he has taught me what it means to be a scientist and medical physicist, how to collaborate with clinicians and other scientists to promote the success of all parties, and the importance of leadership skills at my institution and beyond.

One of my first mentors at the MD Anderson Cancer Center was Dr. Kendra Woods. I am incredibly grateful for the guidance and advice she has provided over the years. Her continued reminders that my personal life and health were just as important as my academic goals helped me remain grounded through the ups and downs of my research.

I have had the pleasure of working with and being mentored by others as well. Dr. Uwe Titt, Dr. Dragan Mirkovic, and Dr. David Grosshans have continually been invested in my success

and I have been able to gain a vast amount of knowledge from them over the years. Dr. David Followill, Dr. Arvind Rao, and Dr. Ronald Zhu have been invaluable members of my advisory committee, always willing to contribute to constructive discussion of my project.

I am greatly appreciative of my funding sources throughout my time in graduate school. These include The University of Texas Graduate School of Biomedical Sciences at Houston, NCI Program Project Grants 5P01CA021239 and 2U19CA021239, the Howard Hughes Medical Institute Med-Into-Grad Program, and The University of Texas MD Anderson Cancer Center Sister Institution Network Fund.

I would also like to thank Stefanie Lewis for her support and encouragement throughout my final year of graduate school. When work wasn't going well, I could always look to her for support and to share my feelings. I love you, Stefanie.

ASSESSING THE POTENTIAL CLINICAL IMPACT OF VARIABLE BIOLOGICAL EFFECTIVENESS IN PROTON RADIOTHERAPY

Christopher Ryan Peeler, B.S.

Advisory Professor: Radhe Mohan, Ph.D.

It has long been known that proton radiotherapy has an increased biological effectiveness compared to traditional x-ray radiotherapy. This arises from the clustered nature of DNA damage produced by the energy deposition of protons along their tracks in medium. This effect is currently quantified in clinical settings by assigning protons a relative biological effectiveness (RBE) value of 1.1 corresponding to 10% increased effectiveness compared to photon radiation. Numerous studies have shown, however, that the RBE value of protons is variable and can deviate substantially from 1.1, but experimental data on RBE and clinical evidence of its variability remains limited.

The potential for using the variable RBE of proton radiation to improve clinical treatment plans has been theorized, but it is accepted that more experimental in vitro and in vivo data are needed before clinical adaptation of these techniques may occur. Nevertheless, it will be important to identify strategies in which the variable nature of proton RBE may be used to inform treatment planning. The goal of this work is thus to investigate if the assumption of a constant proton RBE has an adverse effect in current clinical applications and if the variable biological effectiveness of protons can be quantified from clinical data.

First, results from high-resolution experiments quantifying proton RBE are compared to multiple models for calculating RBE. A new model is then proposed which can more accurately reproduce the experimental results. These models are implemented in a Monte Carlo-based dose calculation system and their output is compared for a cohort of pediatric patients treated for

brain tumors with proton radiotherapy who subsequently presented with post-treatment image changes identified on magnetic resonance imaging. One RBE model is identified as the best candidate for further study; however, results of volumetric analyses of RBE-weighted dose prove inconclusive in correlating with image changes. A model is developed that can describe the probability of voxel-level image changes (signifying normal tissue damage) based on proton dose and linear energy transfer. The model constitutes the first clinical evidence for the variable biological effectiveness of protons and holds promise for the improvement of proton therapy treatment planning.

Table of Contents

Approval Sheet.....	i
Title Page	ii
Dedication	iii
Acknowledgements	iv
Abstract.	vi
Table of Contents	viii
List of Illustrations	xi
List of Tables	xii
Abbreviations	xiii
Chapter 1: Introduction.....	1
1.1. Proton Therapy.....	1
1.2. LET Calculation in Proton Therapy	4
1.3. Relative Biological Effectiveness	5
1.4. Variable RBE Models	8
1.5. The General Radiation Dose-Response Model	14
1.6. Patient Cohort of Interest	16
1.7. Scope of Dissertation	17
Chapter 2: Comparison of Experimental Results and RBE Models.....	20
2.1. Motivation	20
2.2. Methodology	21
2.2.1. MD Anderson Experimental Data	21
2.2.2. Variable RBE model implementation.....	23
2.2.3. Fitting a new RBE model based on MD Anderson experimental data	25

2.3.	Results	26
2.4.	Conclusions	29
Chapter 3:	Comparison of RBE Models for Treatment Plans	31
3.1.	Motivation	31
3.2.	Methodology	32
3.2.1.	Treatment Plans of Interest	32
3.2.2.	Computing Treatment Plans with MCNPX	32
3.2.3.	Computing Variable RBE with MC data	33
3.2.4.	Comparison of Constant and Variable RWD for Treatment Plans	35
3.3.	Results	37
3.4.	Conclusions	39
Chapter 4:	Assessing the Role of Variable Proton Biological Effectiveness in Observed Treatment Outcomes	42
4.1.	Motivation	42
4.2.	Methodology	43
4.2.1.	Patient Cohort and Image Processing	43
4.2.2.	Voxel-level Analysis of Image Changes	44
4.2.3.	Statistical Analysis	44
4.3.	Results	48
4.4.	Conclusions	53
Chapter 5:	General Discussion	55
5.1.	Summary and Discussion of Findings	55
5.2.	Limitations	59
5.3.	Significance and Future Directions	60

Bibliography	64
Vita.....	77

List of Illustrations

1	Proton beamlet depth dose and LET _d for initial beam energies of 79.7 MeV and 219.3 MeV.	2
2	Dose and LET _d for the high-throughput experiment performed at UT MD Anderson Cancer Center.	22
3	Fitting of the ratios α/α_x and β/β_x as functions of LET _d for both the H460 and H1437 cell line experimental results.	27
4	Comparison of measured and model calculated (including new model fit) RBE vs. LET _d for both the H460 and H1437 cell lines.	28
5	TPS and MC dose and dose differences for an example treatment plan.	36
6	Constant RWD, variable RWD, LET _t , and the difference between variable and constant RWD for an example treatment plan.	38
7	Surface plot of generalized linear model for image change based on dose and LET _t	47
8	2-D representations of the generalized linear model for image change for constant LET _t or physical dose.	49
9	TD ₅₀ as a function of LET _t based on interpolation of the generalized linear model for image change.	51
10	Dose, LET _t , and probability of image change distributions for an example patient.	52

List of Tables

1	Equations for RBE_{max} for selected RBE models.....	10
2	Equations for RBE_{min} for selected RBE models.	11
3	Values for RBE_{DSB} and zF obtained from dose averaging of proton energy spectra for cell survival experiment LET_d values.....	24
4	Fitted α_x and β_x parameters and ratios based on Cs-137 cell survival experiments.....	25
5	α_x and β_x parameters and ratios for normal tissues of interest.	34
6	Comparisons of Mean CTV variable and constant RWD for multiple RBE models.	39
7	Univariate and multivariate logistic regression analysis on clinical factors for all patients..	46

Abbreviations

Abbreviation	Meaning
AUC	Area under the curve
CNS	Central nervous system
CT	Computed tomography
CTV	Clinical target volume
DICOM	Digital imaging and communications in medicine
DSB	Double-strand break
FLAIR	Fluid attenuated inversion recovery
ICRU	International Commission on Radiation Units
IMPT	Intensity-modulated proton therapy
LEM	Local effect model
LET	Linear energy transfer
LET _d	Dose-averaged linear energy transfer
LET _t	Track-averaged linear energy transfer
LKB	Lyman-Kutcher-Burman
LOOCV	Leave-one-out cross validation
LQ	Linear quadratic
MC	Monte Carlo
MCDS	Monte Carlo Damage Simulation
MRI	Magnetic resonance imaging
MU	Monitor unit
NTCP	Normal tissue complication probability

PSPT	Passive scattering proton therapy
RBE	Relative biological effectiveness
RBE_{DSB}	Relative biological effectiveness of double-strand break induction
RMF	Repair-misrepair-fixation
ROC	Receiver operating characteristic
RT	Radiotherapy
RWD	Relative biological effectiveness-weighted dose
SOBP	Spread-out Bragg peak
TD	Tolerance dose
TD_{50}	Tolerance dose at which 50% of treated patients would be expected to experience a toxicity
TPS	Treatment planning system

Chapter 1: Introduction

1.1. Proton Therapy

Proton therapy is a radiation treatment modality that first came into use in the 1950s. For many years its use remained limited due to a small number of available facilities; however, recent years have seen a dramatic increase in the number of proton therapy centers across the globe. This increase in adoption is certainly due in part to the physical phenomenon, the Bragg peak, which provides protons a theoretical advantage over other standard photon radiation treatment modalities. As protons travel through a material, such as human tissue, they gradually lose energy through Coulomb scattering and nuclear interactions and the rate of energy loss increases as they slow down. Thus, nearing the end of their range, they rapidly deposit the remainder of their energy in a characteristic Bragg peak, after which the protons essentially stop, leaving little to no dose. This is an appealing characteristic as proper planning would allow one to deliver appropriate proton radiation dose to a tumor while delivering lower dose to the structures proximal to the tumor and also nearly completely sparing the structures distal to the tumor.

Proton's ability to deposit dose at differing rates at different depths is due to the physical property known as linear energy transfer (LET). This value specifically quantifies the rate at which protons transfer their energy to medium and is dependent on the stopping power of a proton which is in turn dependent on the proton energy. As the energy of protons decreases as they traverse a medium, i.e. as they transfer more of their energy to the medium, the stopping power of the protons increases and thus the LET or rate at which the protons transfer their energy increases. Furthermore, while proton dose deposition decreases beyond the Bragg peak, the LET continues to increase with the highest values being achieved beyond the peak. An

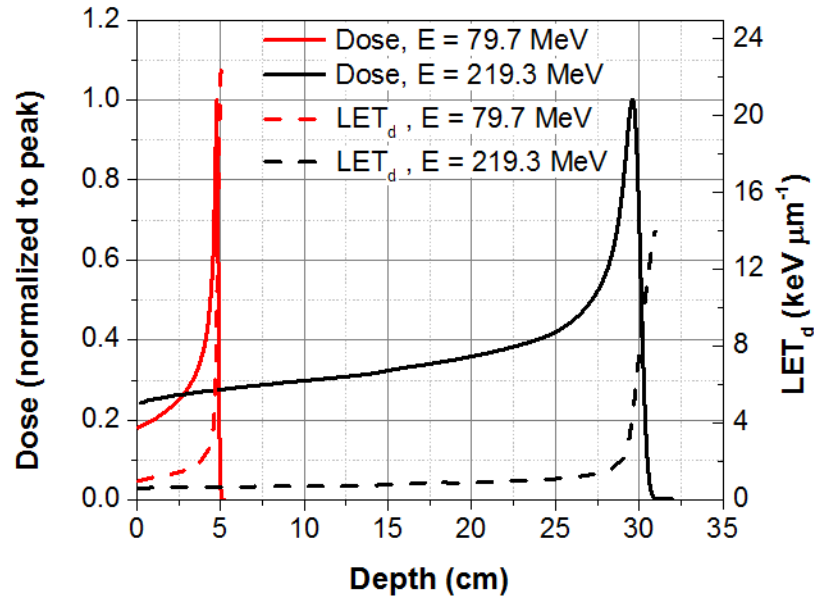


Figure 1: Proton beamlet depth dose and LET_d for initial beam energies of 79.7 MeV and 219.3 MeV.

Proton beamlet depth doses (solid lines) are presented for beamlets with initial energy of 79.7 MeV (red) and 219.3 MeV (black). Corresponding dose-averaged LET (LET_d) is also presented for each beam energy.

example of proton dose and dose-averaged LET (LET_d) profiles in medium for two different initial proton energies is presented as an example in **Figure 1**. The concept of LET_d will be discussed in detail in Section 1.2.

Over the years several different strategies for delivering proton radiation to treat cancer have been developed. The more traditional method of delivery is known as passively scattered proton therapy (PSPT). In this modality, an initial pristine proton beam that has been extracted from a synchrotron or cyclotron is first scattered to create a broad beam¹. After passing through necessary beam monitoring devices, the beam is then spread longitudinally with what is

generally referred to as a range modulator². This device, which may consist of a metal wheel of varying thickness, serves to create what is known as a spread out Bragg peak (SOBP)². The SOBP is designed such that it will uniformly deliver dose over the depth axis of the tumor². The edges of the proton beam are then shaped by a patient specific aperture, and the distal edge of the beam is shaped to the tumor with a patient specific compensator. Multiple beams are normally used in order to reduce the dose received by the normal tissues encountered by the beams. The name and specific design of the various components may differ at each particular treatment facility.

More recent years have seen the rise of a treatment technique known as intensity modulated proton therapy (IMPT) which has been made possible by increases in available computational power and advancements in the technology itself. In IMPT the range modulator and compensator components of the beamline are omitted. Instead, numerous “pristine” Bragg peaks are used to deliver radiation dose to the tumor^{3,4}. Energy modulation, i.e. a sequence of beam energies, is used to vary the range of the individual beamlets while steering magnets are used to determine their lateral placement^{3,4}. Collectively, the dose from the beamlets, normally impinging from two or more beam directions, results in the delivery of the prescribed dose⁵.

IMPT is the more powerful form of proton therapy due to its ability to provide improved normal tissue sparing. This benefit, however, comes at the cost of greater vulnerability to uncertainties with the loss of homogeneity of individual beams and the potential for dose “hot spots”, focal areas of increased dose, within the target^{6,7}. It may also result in the shifting of higher LET components of individual beams into locations that they may not have appeared previously^{8,9}. This could potentially become an issue when one considers that the LET characteristics of protons result in an increased capability for cell kill compared to photon radiation¹⁰⁻¹².

1.2. LET Calculation in Proton Therapy

In order to properly quantify any increased capability for cell kill for proton beams, it is first necessary to be able to accurately calculate the LET of protons. While an individual proton may have an LET value at a given location, it is often necessary and more practical to consider an average value over many protons traversing an area or volume. A method for calculating LET as a weighted average over different quantities has been described by Wilkens and Oelfke¹³. According to their method, LET at a given depth or location may be calculated either as a track- or fluence-averaged quantity or as a dose-averaged quantity over protons of all residual ranges at that location. In a publication by Guan and Peeler et al.¹², the formalism by Wilkens and Oelfke¹³ was rewritten in terms of proton energy instead of residual range, though these are essentially equivalent as the residual range corresponds to a proton energy. The track-averaged LET (LET_t) may thus be calculated according to

$$LET_t(z) = \frac{\int_0^\infty S_{el}(E)\phi(E,z)dE}{\int_0^\infty \phi(E,z)dE} \quad (1)$$

where in the numerator, the product of the electronic stopping power (S_{el}) and fluence (ϕ) for a given proton energy are integrated over all protons of all energies at the location z along the depth¹². The denominator is the sum of the fluences of all protons of all energies at that location, which is simply the total fluence. Thus, the quantity is averaged over the fluence, lending to the “fluence-averaged” designator; however, this quantity is often referred to as the LET_t in practice^{12,13}. The dose-averaged LET (LET_d) may be calculated in a similar manner according to

$$LET_d(z) = \frac{\int_0^\infty S_{el}(E)D(E,z)dE}{\int_0^\infty D(E,z)dE} \quad (2)$$

where $D(E,z)$ is the dose from a given energy of protons, E , at a location, z ¹². The dose is a function of the electronic stopping power and fluence given by

$$D(E,z) = \frac{S_{el}\phi(E,z)}{\rho(z)} \quad (3)$$

where $\rho(z)$ is the density of the medium at location z ¹². At any given location, the values for LET_t and LET_d will vary depending on the spectrum of proton energies present; however, as indicated by Guan and Peeler et al. the differences between LET_t and LET_d most notably occur near the end of the proton range in the region at or beyond the Bragg peak¹². It is in this region that the LET_t provides an underestimation compared to the LET_d . In low LET regions, the values of the two quantities are observed to agree well¹².

For the purposes of this study, LET_t and LET_d are both utilized in differing situations primarily according to the data available to perform the calculations. In particular, LET_d requires decoupled energy spectrum and fluence data in order to properly perform the dose-averaging operation. It is thus necessary to consider where these two quantities are equivalent and not equivalent when evaluating the results. In either case, the average LET has generally been considered an acceptable surrogate for the biological effectiveness of protons and most of the published work on this topic has relied on average LET values. Increasingly, however, averaged LET is being realized to be a less accurate index of biological effect.

1.3. Relative Biological Effectiveness

It has long been known that light and heavy ions have an increased biological effect in tissue compared to traditional photon treatment modalities. This increased effectiveness is known as the relative biological effectiveness (RBE), which refers to the relative increase in the capability for cell kill of an ion or other modality compared to a traditional photon based modality, such as x-rays or Co-60 gamma rays. It is specifically defined as the ratio of a reference photon dose to

the dose of a radiation type/quality of interest that results in the same biological effect and is represented by the following equation

$$RBE = \frac{D_x}{D_t} \quad (4)$$

in which D_x is the reference photon dose and D_t is the dose of a test radiation of interest (henceforth D_t will be referred to as D_p because this study focuses specifically on protons). The reason for this increased RBE for ions lies in the nature of their energy deposition, specifically that it is concentrated along the ion track leading to more localized DNA damage and a higher number of complex double strand breaks (DSBs)¹⁴. For protons, the value of the RBE has long been assumed to be 1.1 meaning that protons are 10% more effective than photons with regard to killing cells. The selection of this value was largely determined based on in vitro experimental data and limited in vivo data; however, based on this same data, the value is known to vary from 1.0 to as high as 3.0 or even higher in some cases^{11,15–20}. Despite this fact, the International Commission on Radiation Units (ICRU) recommends that a constant value of 1.1 be used as the RBE of protons for the purposes of clinical treatment planning and delivery due to a lack of convincing clinical evidence to support the use of other values²¹.

The more recent comprehensive assessments of proton RBE have been conducted by Paganetti et al.^{18,20} His 2002 study aimed to collect and summarize much of the accumulated knowledge of proton RBE and make some assessment as to how the information should be utilized moving forward. This work reaffirmed the fact that proton RBE may vary around the accepted value of 1.1 and also noted that underestimations of the RBE on the order of 10% could present clinically significant consequences¹⁸. In 2014, Paganetti again performed a comprehensive review of the available experimental data for proton RBE²⁰. This study collected and evaluated 369 data points from proton cell survival experiments obtained from 76 publications²⁰. Beyond simply summarizing results, Paganetti's study in some cases provided

newly calculated LET values when they were unavailable in the original publication. The end result was a thorough view of the published results of proton RBE for a range of clinically relevant LET values. The results were summarized by stating that the RBE of protons varies from 1.1 in the entrance/plateau region ranging up to 1.35 at the distal edge of the Bragg peak. The average value reported for the distal falloff region was 1.7²⁰. This study underlines the continual importance of the evaluation of new literature and also the value of more experimental data in contributing to the overall knowledge of proton RBE.

A more recent set of published results is of additional interest. A study by Chaudhary et al.¹¹ evaluated proton RBE through cell survival experiments in a consistent and thorough manner for both a pristine Bragg peak and an SOBP¹¹. Experiments were performed for both the AG01522 normal human skin fibroblast cell line and U87 radioresistant human glioma cell line¹¹. RBE values were measured for a range of positions along the beam depth dose profiles corresponding to LET_d values up to ~25 keV μm^{-1} . For a cell surviving fraction of 10%, RBE values between 2.0 and 2.5 were reported for LET_d values of 20-25 keV μm^{-1} ¹¹. Such LET_d values are high and would typically be encountered in the distal falloff region, but this remains of relevance because this region of the proton depth dose distribution often deposits energy in normal tissue structures beyond the tumor target. The observed high RBE values are thus of concern with regard to traditional treatment planning techniques and the potential for high RBE protons to deposit dose outside of the target.

It is still believed that the current experimental knowledge of proton RBE is not sufficient to make sweeping changes to the standard of practice of constancy of RBE and clear clinical evidence would be required to provide sufficient impetus for change¹⁸. The aim of this work is thus not to directly suggest altering current clinical practice, but rather to determine if clinical

evidence supporting the use of variable RBE can be extracted from current outcomes observed in proton therapy.

1.4. Variable RBE Models

In more recent years, various groups have investigated and implemented means of accounting for the variable nature of proton RBE in dose calculation²²⁻²⁸. This has led to the development of several different methods of calculating or accounting for proton RBE, each of which assumes a different name. Such methods, however, may collectively be referred to as variable RBE models: models which accept various forms of input data to calculate proton RBE at any particular point of dose calculation. The primary basis for these models is a radiobiological model known as the linear-quadratic (LQ) model. This model describes the nature of the response of living cells to radiation. For a given type of radiation, a plot of cell surviving fraction (SF) with respect to delivered radiation dose (D) may be represented by

$$SF = e^{-\alpha D - \beta D^2} \quad (5)$$

in which α and β are coefficients specific to the type of cells being irradiated. The coefficients are generally determined by fitting the results of clonogenic cell survival experiments with the model. According to the definition of RBE, the LQ equations for survival fraction for the reference photon dose and proton dose may be used to solve for the ratio of these doses.

Simplifying the result provides the following equation

$$RBE = \frac{D_x}{D_p} = \frac{\sqrt{\alpha_x^2 + 4\beta_x D_p (\alpha + \beta D_p)} - \alpha_x}{2\beta_x D_p} \quad (6)$$

in which α_x and β_x are the biological coefficients for photons and α and β are the coefficients for protons²². This equation thus provides a means to calculate RBE as a function of photon and

proton biological coefficients and proton dose. It is important to note, though, that the published data for the biological coefficients for protons is limited.

Carabe-Fernandez et al.^{27,28} later proposed a new parameterization of the basic RBE model incorporating the concepts of an RBE_{max} and RBE_{min} . These are asymptotic relationships based on either the dose approaching zero or infinity, respectively. RBE_{max} is represented by

$$RBE_{max} = \frac{\alpha}{\alpha_x} \quad (7)$$

where dose is assumed to approach zero. RBE_{min} is represented by

$$RBE_{min} = \sqrt{\frac{\beta}{\beta_x}} \quad (8)$$

where dose is assumed to approach infinity. In order to incorporate this concept into the RBE model in **Equation (6)**, the model must first be rewritten in terms of the ratios of the α and β values. The resulting formula is represented by **Equation (9)**

$$RBE = \frac{D_x}{D_p} = -\frac{1}{2D_p} \left(\frac{\alpha}{\beta} \right)_x + \frac{1}{D_p} \sqrt{\frac{1}{4} \left(\frac{\alpha}{\beta} \right)_x^2 + \frac{\alpha}{\alpha_x} \left(\frac{\alpha}{\beta} \right)_x D_p + \frac{\beta}{\beta_x} D_p^2} \quad (9)$$

which is now also written in terms of the ratio of α_x and β_x ^{27,29}. All of the models used in this study are thus rewritten to follow this standard form as in many cases it removes the dependence on proton α and β values.

Six published models for proton RBE will be used for the analysis in this study. The RBE_{max} and RBE_{min} parameterizations for all of the models are presented in **Table 1** and **Table 2**, respectively. The first model to be discussed may be referred to as the phenomenological model or the Wilkens and Oelfke model after the scientists that proposed it²². The objective in the development of this model was to create something based on the linear-quadratic model and that could be fitted and tested according to existing experimental results²². Given that biological factor data for reference x- ray radiation is more abundant than that for protons, it was deemed

Table 1: Equations for RBE_{\max} for selected RBE models.

The RBE_{\max} formalisms for six selected RBE models are collected here. In some cases the equations have been rewritten from the originally published form to match the RBE_{\max} definition.

Model	$RBE_{\max} \left(\frac{\alpha}{\alpha_x} \right)$	Equation #
Wilkins and Oelfke ^{22,30}	$1 + \frac{\lambda}{\alpha_x} (LET_d - 0.5 \text{ keV } \mu\text{m}^{-1})$	(10)
Wedenberg et al. ²⁵	$1 + \frac{0.434}{(\alpha/\beta)_x} LET_d$	(11)
Carabe-Fernandez et al. ^{27,28,31}	$0.843 + 0.154 \frac{2.686}{(\alpha/\beta)_x} LET_d$	(12)
McNamara et al. ³²	$0.999064 + \frac{0.35605}{(\alpha/\beta)_x} LET_d$	(13)
Chen and Ahmad ²⁶	$\frac{1}{\alpha_x} \left(0.1 + \frac{1 - e^{-0.0013 LET_d^2}}{0.045 LET_d} \right)$	(14)
RMF ^{23,24,29,33}	$RBE_{DSB} \left(1 + \frac{\bar{z}_F RBE_{DSB}}{(\alpha/\beta)_x} \right)$	(15)

prudent to parameterize this equation to depend only on coefficients for x-rays²². It was identified that a linear relationship based on the LET_d of protons could be used to relate the proton α value to that of x-rays based on experimental data for V79 Chinese hamster cells from studies by Goodhead et al.³⁴, Blomquist et al.³⁵, Belli et al.^{10,15}, Folkard et al.³⁶, Wouters et al.¹⁶, and Schettino et al.³⁷ A linear scaling factor λ is used to describe the change in the proton α with LET_d . Very little conclusive data regarding the β coefficient for protons is available, so it was deemed best to

Table 2: Equations for RBE_{min} for selected RBE models.

The RBE_{min} formalisms for six selected RBE models are collected here. Values of 1 indicate that the β for protons was assumed to be equal to that of photons.

Model	$RBE_{min} \left(\sqrt{\frac{\beta}{\beta_x}} \right)$	Equation #
Wilkens and Oelfke ²²	1	(16)
Wedenberg et al. ²⁵	1	(17)
Carabe-Fernandez et al. ^{27,28,31}	$1.09 + 0.006 \frac{2.686}{(\alpha/\beta)_x} LET_d$	(18)
McNamara et al. ³²	$1.1012 - 0.0038703 \sqrt{(\alpha/\beta)_x} LET_d$	(19)
Chen and Ahmad ²⁶	1	(20)
RMF ^{23,24,29,33}	RBE_{DSB}	(21)

simply set it equal to the β value for x-rays²². In practice this model has been shown to reasonably replicate experimental data and has also been applied to calculate RWD distributions for individual treatment plans^{22,30,38}. The representation of the model in **Equation (10)** is adapted from that presented by Frese et al.³⁰ Using the equations

$$\alpha = \alpha_0 + \lambda * LET_d \quad (22)$$

$$\alpha_0 = \alpha_x - 0.5 \frac{keV}{\mu m} * \lambda \quad (23)$$

where α_0 is the initial α value or intercept, **Equation (23)** is substituted into **Equation (22)**. The resulting equation is then divided by α_x in order to produce an equation representative of RBE_{max} which is **Equation (10)**³⁰.

Another similar linear model of RBE_{\max} with LET was published by Wedenberg et al.²⁵ In their model, α/α_x was fit as a linear function of LET, but the scaling parameter was written as an inverse relationship with $(\alpha/\beta)_x$, such that for high values of $(\alpha/\beta)_x$ the calculated RBE would be less dependent on LET²⁵. Analysis of previously published experimental data again led to the use of an RBE_{\min} value of 1²⁵. The RBE_{\max} and RBE_{\min} formalisms for this model are presented in **Equations** (11) and (17).

The model by Carabe-Fernandez et al.³¹ was also determined through linear regression analysis of the results of previously published experiments. The fitting was performed over data from many of the same experiments employed by Wilkens and Oelfke²² with additional data from Coutrakon et al.³⁹ The exact form used for this work was published by Carabe-Fernandez et al. in 2012³¹. The models for RBE_{\max} and RBE_{\min} both scale linearly with LET_d with the scaling term being inversely proportional to $(\alpha/\beta)_x$. RBE_{\max} and RBE_{\min} are represented by **Equations** (12) and (18), respectively.

The last of the included models with a similar linear form for RBE_{\max} and RBE_{\min} is that by McNamara et al.³² Fitting of this model was performed over 287 experimental data points collected over numerous experiments in a review by Paganetti²⁰. The resulting model for RBE_{\max} was a linear function of LET with the scaling term inversely proportional to $(\alpha/\beta)_x$ ³². The equation for RBE_{\min} was also linear with LET; however, in this case the scaling term was directly proportional to $\sqrt{(\alpha/\beta)_x}$ ³². The formalisms for RBE_{\max} and RBE_{\min} are represented by **Equations** (13) and (19).

A nonlinear model describing the change in α with LET for protons was described by Chen and Ahmad²⁶. This model was fit based on data from Wouters et al.¹⁶, Belli et al.^{10,15}, and Folkard et al.³⁶ and captured the observed decrease in α for high values of LET. The value of β for protons was assumed to be a constant for the sake of simplicity²⁶. The model did not

incorporate scaling based on $(\alpha/\beta)_x$. The resulting equations with the fitted parameters are presented by **Equations** (14) and (20).

Another model that is based more directly on the biological mechanisms involved in radiation damage is known as the repair-misrepair-fixation (RMF) model^{23,24,33}. The name is descriptive of the biological processes that are accounted for within the model. The model as it is employed for this work is based on the concept of RBE of DSB induction (RBE_{DSB}) employed by Polster et al.²⁹ for implementation of the model into a Monte Carlo calculation framework. RBE_{DSB} is an extension of the definition of RBE to the relative number of DSBs induced by proton radiation compared to photon radiation for different proton radiation quality. The total number of DSBs generated in a cell by a given radiation quality is represented by the symbol Σ . The RBE_{DSB} can thus be represented by the equation

$$RBE_{DSB} = \frac{\Sigma_p}{\Sigma_x} \quad (24)$$

where Σ_p is the number of DSBs per Gray per giga base pair ($DSB\ Gy^{-1}\ Gbp^{-1}$) for protons and Σ_x is the $DSB\ Gy^{-1}\ Gbp^{-1}$ induced by photons for a given dose. Values for Σ may be obtained using the Monte Carlo Damage Simulation (MCDS) software developed by Semenenko et al.^{24,40-43} This software serves to rapidly model the biological processes of DNA damage, repair, misrepair, and fixation in order to determine a total number of DSBs produced by a given radiation quality. **Equations** (15) and (21) present the models for RBE_{max} and RBE_{min} as they are implemented in this work. The term \bar{z}_F in **Equation** (15) is the frequency-mean specific energy which is a microdosimetric term analogous to energy deposition or dose²³. The model has been shown to agree reasonably well with lower ion LET values, such as those that would be encountered in proton therapy^{23,24,43}.

Another model worth noting briefly is known as the local effect model (LEM). This model was developed by Scholz and Kraft et al., building from an earlier model from Butts and Katz et

al., to address the issue of accurately accounting for RBE-weighted dose (RWD) for carbon ion therapy⁴⁴⁻⁴⁷. The LEM model is based primarily on the radial dose deposition from ion tracks and uses this and information of track structure to determine the amount and location of DNA damage that occurs from a summation of individual tracks^{46,47}. This model is not as readily applicable for this study and thus will not be explored further.

1.5. The General Radiation Dose-Response Model

In the realm of photon therapy, the appropriate safe and effective doses used for patient treatment have largely been determined based on retrospective analyses of observed treatment outcomes. The large collection of outcomes data obtained from many years of photon radiotherapy have been employed for the purpose of building models to describe the relationship of the delivered dose with both tumor and normal tissue response. Such models are referred to as dose-response models, and a large collection of such models have been developed over the years.

Some of the earliest and subsequently most cited work in this field was published by Lyman in the 1980s⁴⁸. Based on treatment outcome data, Lyman developed a model to describe normal tissue response based on volumes of delivered dose in organs of interest. The probability of response predicted by the model is known as normal tissue complication probability (NTCP). The model developed by Lyman is based on the sigmoid-shaped curve produced by the probit function represented by **Equation (25)**.

$$P = F(c|\mu, \sigma) = \frac{1}{\sigma\sqrt{2\pi}} \int_{-\infty}^c e^{-\frac{(c-\mu)^2}{2\sigma^2}} dc \quad (25)$$

Assuming mean $\mu = 0$ and standard deviation $\sigma = 1$ results in the following equation

$$P = F(c) = \frac{1}{\sqrt{2\pi}} \int_{-\infty}^c e^{-\frac{c^2}{2}} dc \quad (26)$$

which is the form of the equation employed by Lyman⁴⁸. Lyman parameterized the exponent of this model in terms of the tolerance dose (TD) at which a percentage of patients receiving that dose to a given volume of tissue would be expected to experience a certain response or complication. The TD at which 50% of patients would be expected to experience a complication would be abbreviated as TD₅₀, for example. Lyman's parametrization of the exponent of the probit function is represented by

$$c = \frac{D - TD(V)}{m * TD(V)} \quad (27)$$

where D is the delivered dose and m is a parameter that characterizes the slope of the probit curve⁴⁸. TD(V) describes the TD for a specific uniformly irradiated partial volume (V) of the anatomic structure. TD(V) may be determined according to

$$TD(V) = \frac{TD(1)}{V^n} \quad (28)$$

where TD(1) is the TD for uniform irradiation of a whole organ volume, V is the irradiated volume of interest and n is a fitted parameter based on outcomes data for different organs⁴⁸.

This model was later expanded upon by Kutcher and Burman who developed the strategy to compute the equivalent uniformly irradiated partial volume from an arbitrary non-uniform irradiation⁴⁹. They also applied the model for fitting of collected outcomes data presented by Emami et al.⁵⁰ and recorded the model parameters for 28 organs of interest constituting 29 different endpoints⁵¹. The more modern form of the model is referred to as the Lyman-Kutcher-Burman or LKB model.

1.6. Patient Cohort of Interest

One of the inherent physical advantages of proton therapy is its lack of exit dose and low entrance dose compared to the dose delivered at the target location. In general the doses delivered to normal tissues in proton therapy are low compared to photon therapy due to the proton physical properties. Such properties may be of special benefit for brain tumors in pediatric patients requiring radiotherapy, where low dose radiation exposure, seen even with advanced photon techniques, may be associated with significant radiation induced adverse effects, such as cognitive decline^{52,53}. It is thus of great interest to physicians when unexpected levels of adverse treatment effects are observed in this subset of patients, as the prevailing thought is that proton therapy should be the more favorable treatment modality⁵⁴⁻⁵⁷.

A more recently published study by Gunther et al. observed that for a cohort of pediatric patients treated for brain tumors, specifically ependymoma, the patients treated with protons presented with post-treatment image changes on follow-up MRI at a higher rate than those patients treated with photons⁵⁸. These patients were treated on a prospective protocol comparing normal tissue toxicity between intensity-modulated photon therapy (IMRT) to PSPT. Radiotherapy type, months after surgery before radiotherapy, age at radiotherapy, and an interaction variable for radiotherapy type and age were examined on multivariate logistic regression analysis to determine association with the development of image changes⁵⁸. The radiotherapy type (proton therapy) was found to be the only significant factor ($p = 0.024$) associated with the development of image changes⁵⁸.

One of the most identifiable physical differences between proton and photon therapy is the nature of the LET of the modalities. Proton LET is not constant along the proton beam path and is known to contribute to a variable biological effectiveness compared to photons. It is thus of interest to study this particular cohort of patients due to their high rate of observed post-

treatment normal tissue effects in order to better understand if or how they are related to the physical and biological properties of proton radiotherapy.

1.7. Scope of Dissertation

The RBE of protons for radiotherapy is traditionally assigned a constant, average value of 1.1; however, the actual RBE of protons varies over the deposited dose distribution based on various factors, including proton energy, LET, dose per treatment fraction, number of treatment fractions, tissue and cell type specific factors, and biological and clinical endpoints. It is plausible that the use of an average RBE value may lead to unexpected areas of higher effective dose and subsequent normal tissue toxicity. Variability in RBE may be accounted for by incorporating a model that applies an RBE value determined by the factors specific to each point in the patient dose calculation grid. This model may assume many forms, and indeed many models have been previously published. It is important to remember, though, that the tissue specific biological factors incorporated into such models are inherently prone to uncertainty due to the limited amount of in vitro and in vivo data available, a fact which must be considered when evaluating biologically weighted treatment plans. Despite the current limitations, it will be increasingly important to identify strategies in which the growing knowledge of proton RBE may be utilized to improve the standard of care in proton therapy. **The central hypothesis of this work is that radiation-induced imaging changes in the brain and brainstem resulting from proton radiotherapy are associated with the variable biological effectiveness of protons.** The hypothesis is tested for a cohort of pediatric patients treated for ependymoma who subsequently presented with radiation-induced imaging changes on post-treatment scans. The means of testing this hypothesis are encompassed by the following specific aims.

Specific Aim 1: *To determine if the predictions of current RBE models are consistent with the results of high-throughput, high-resolution in vitro proton irradiation cell survival experiments.* Radiobiological modeling is performed for the results of cell survival experiments conducted with a high-resolution experimental system developed at the UT MD Anderson Cancer Center. Models and experimental results are compared to assess the accuracy of the models for the system. A new model is proposed when the current models are unable to adequately predict the results.

Specific Aim 2: *To determine if there is a clinically significant difference between RBE-weighted proton treatment plan dose distributions calculated using different RBE models.* A collection of current proton RBE models are incorporated into an in-house Monte Carlo dose calculation framework. For a collection of treatment plans, this provides un-weighted dose, track-averaged linear energy transfer, and RBE and RWDs from multiple models on a voxel-by-voxel basis. Dose distributions determined with each model are evaluated for differences and any trends noted over a collection of patients. The best model for further analysis is identified.

Specific Aim 3: *To determine if the spatial location of proton radiation induced imaging changes is associated with the variable biological effectiveness of proton radiotherapy.* For a cohort of pediatric ependymoma patients treated with passive scattering proton therapy, Monte Carlo calculated treatment plans incorporating metrics describing variable proton biological effectiveness are analyzed. Treatment plans for patients presenting with radiation-induced post-treatment imaging changes are compared against those of patients without imaging changes to determine if changes are associated with variable biological effectiveness. A practicing radiation oncologist identified and contoured regions of image change on treatment planning computed tomography (CT) images using co-registered post-treatment MRI sequences. The

image change contours are used to determine if the spatial location of changes coincides with increased variable biological effectiveness as opposed to constant biological effectiveness.

Chapter 2: Comparison of Experimental Results and RBE Models

2.1. Motivation

Specific Aim 1: To determine if the predictions of current RBE models are consistent with the results of high-throughput, high-resolution in vitro proton irradiation cell survival experiments.

As has been previously discussed, there are many published models for proton RBE. Some of them are based on differing approaches to fitting similar experimental data, while others are based on different approaches altogether to representing the biological effects of protons. Due to these differences, the models provide different predictions of proton RBE and it is thus worthwhile to quantify how effective they are in modeling what is considered to be highly accurate experimental data.

The proton biological effects research group at MD Anderson has produced a robust dataset that provides high-resolution data for RBE as a function of LET_d ¹⁹. Most previously published experimental RBE datasets have been based on measurements in SOBPs. The energy spectrum of protons in an SOBP is generally rather broad and much less sharp than the spectrum that would be observed in a pristine Bragg peak¹⁹. As a result, the previous experiments are more relatable to average LET_d values as opposed to a single LET_d value. While the LET_d value at a given point in a pristine Bragg peak is still an average, the reduced width of the energy spectrum is considered to provide a more accurate representation of the RBE for a given LET_d .

The goal of the analysis here is to apply the published RBE models previously discussed to determine if their predictions are still valid for high-resolution RBE data based on measurements in pristine Bragg peaks. Invariably, the published models have provided for a linear increase of RBE with LET_d . The published RBE data from the MD Anderson group's

experiments exhibit a non-linear increase in RBE particularly for LET_d values above $\sim 10 \text{ keV } \mu\text{m}^{-1}$ ¹⁹. In order to properly account for this difference in the high LET region moving forward, a new model will be fit that is nonlinear in design while at the same time being scaled based on the $(\alpha/\beta)_x$ to account for the inherent differences in biological response of different cell lines.

2.2. Methodology

2.2.1. MD Anderson Experimental Data

In an effort to better define proton RBE for various levels of proton LET, the group at MD Anderson designed an experiment in order to measure cell survival for different levels of dose and LET for an “IMPT-like” beam. The experimental setup has been described in detail in the publication by Guan and Bronk et al.¹⁹ The design consisted of a stepped compensator made of Lucite, which was placed in the path of the beam proximal to a 96-well plate. The proton gantry was placed in the 180° position, i.e. below the compensator and plate with the beam directed upward. The result of this setup was that the different columns of the 96-well plate were irradiated with different parts of the Bragg curve and thus encountered different levels of dose and LET. The relative dose and LET values for each column of the 96-well plate are presented in **Figure 2**.

After irradiation the samples were processed in order to produce cell survival curves based on the clonogenic survival assay. The experimental data presented for this work consisted of two repeat experiments with the H460 cell line and also two repeat experiments with the H1437

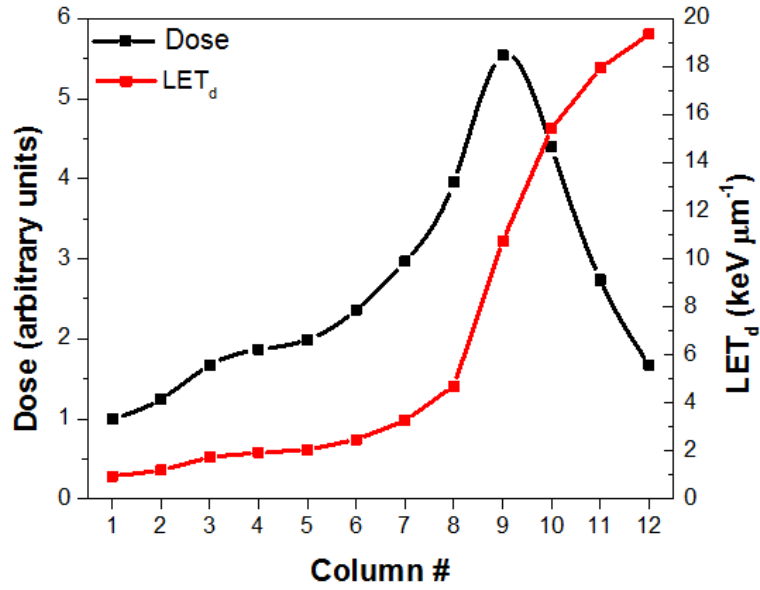


Figure 2: Dose and LET_d for the high-throughput experiment performed at UT MD Anderson Cancer Center.

Dose and LET_d in each of the 12 columns of the 96-well plate for the high-throughput clonogenic survival experiments performed at UT MD Anderson Cancer Center. Dose and energy spectra data were calculated by Fada Guan, Ph.D., using the Geant4 Monte Carlo code¹⁹.

cell line. Both lines are non-small cell lung cancer cell lines. Experiments were performed by Lawrence Bronk at the Proton Therapy Center – Houston¹⁹. A reference data set was produced by irradiating the cell lines with Cs-137 photons. The survival curves for the photon irradiation were used in the determination of RBE of protons compared to photons. For this work, LET_d values were calculated according to **Equation (2)** in which the LET is a dose-averaged quantity. In order to calculate the RBE values, the survival curves were fit using the LQ model (**Equation (5)**) to obtain the α and β values for each of the different proton LET_d values for which measurements were performed. Equivalent photon and proton doses required to achieve a SF of 10% were then calculated for each measurement point. This allowed for the generation

of proton α and β values as a function of LET_d as well as RBE for 10% SF as a function of LET_d for both H460 and H1437 cell lines.

2.2.2. Variable RBE model implementation

Six previously published models for variable proton RBE were selected for comparison in this study. These include the models by Wilkens and Oelfke²², Wedenberg et al.²⁵, Carabe-Fernandez et al.^{27,28,31}, McNamara et al.³², Chen and Ahmad²⁶, and the RMF model^{23,24,29,33}. All of the models can be represented by the same basic LQ relationship represented by **Equation (9)**. The parameterizations of each of the different models in terms of RBE_{max} and RBE_{min} were previously presented in **Table 1** and **Table 2**, respectively. All of the models are based on LET_d , which was calculated according to **Equation (2)** presented in Section 1.4 using proton energy spectrum data obtained through Geant4 Monte Carlo calculations performed by Fada Guan, Ph.D¹⁹. As described in Section 2.2.1, reference photon α_x and β_x values were determined by fitting of Cs-137 clonogenic survival experiment results. These values were then incorporated into the RBE calculation.

An additional parameter was required for the calculation of RBE with the model by Wilkens and Oelfke. The parameter λ , the LET scaling term, was determined according to the method described by Frese et al. in which α_x , β_x , the average target dose per fraction and the average target LET_d were used to calculate the λ value necessary to achieve an average RBE of 1.1 in the target. **Equation (29)** describes this method

$$\lambda_{1.1} = \frac{\alpha_x(RBE - 1) + \beta_x \bar{D}(RBE^2 - 1)}{\bar{L} - 0.5 \text{ keV}/\mu\text{m}} \quad (29)$$

where \bar{D} is the average dose per fraction in the target and \bar{L} is the average LET^{30} . Based on the experimental data, λ was calculated to be $0.02 \mu\text{m keV}^{-1} \text{ Gy}^{-1}$ for a dose of 3 Gy, corresponding

Table 3: Values for RBE_{DSB} and \bar{z}_F obtained from dose averaging of proton energy spectra for cell survival experiment LET_d values.

Dose-averaged RBE_{DSB} and \bar{z}_F (frequency mean specific energy) are presented for each of the LET_d values for which measurements were made in the high-resolution cell survival experiments.

LET_d (keV μm^{-1})	RBE_{DSB}	\bar{z}_F (Gy)
0.94	1.02	0.008
1.19	1.02	0.010
1.74	1.04	0.014
1.93	1.05	0.016
2.04	1.05	0.017
2.48	1.06	0.020
3.26	1.09	0.027
4.71	1.13	0.038
10.7	1.34	0.086
15.4	1.49	0.123
17.9	1.57	0.142
19.4	1.62	0.153

to 10% SF, for LET_d of 4.7 keV μm^{-1} so that an RBE of 1.1 was achieved at this point. This point was selected to provide acceptable matching to the experimental data.

In order to calculate RBE based on the RMF model, proton energy spectra for each LET_d value were used to dose average the quantities RBE_{DSB} and \bar{z}_F . Dose averaging was performed in a manner similar to that presented for LET in **Equation (2)**. In this case $\text{RBE}_{\text{DSB}}(\text{E})$ or

Table 4: Fitted α_x and β_x parameters and ratios based on Cs-137 cell survival experiments.

LQ model parameters for the H460 and H1437 cell lines obtained from fitting with the LQ model are presented. Standard deviations are included in parentheses.

Cell Line	α_x	β_x	$(\alpha/\beta)_x$
H460	0.36 (± 0.03)	0.071 (± 0.008)	5.1 (± 0.7)
H1437	0.08 (± 0.03)	0.031 (± 0.005)	3 (± 1)

$\bar{z}_F(E)$ was substituted for $S_{el}(E)$ in the numerator. A Σ_x value of 8.3 DSB Gy⁻¹ Gbp⁻¹ for Cs-137 γ -rays was utilized for the calculation of RBE_{DSB}. The obtained values used for RBE calculation are presented in **Table 3**.

2.2.3. Fitting a new RBE model based on MD Anderson experimental data

Given the non-linear increase of RBE with LET_d in the MD Anderson experimental results, a new variable RBE model was also fit to the data. The approach taken for fitting the model was similar to that seen in previous publications in that the ratio α/α_x and $\sqrt{\beta/\beta_x}$ were fit as functions of LET_d with dependence on $(\alpha/\beta)_x$ to provide additional scaling based on the inherent biological properties of different cell lines. The polynomial form chosen for fitting was that of the cubic function due to the substantial non-linear increase in the ratios for the highest LET values as observed in the study by Guan and Bronk et al.¹⁹ Fitting was performed using the nonlinear regression toolbox of OriginLab 8.6 (OriginLab Corporation, Northampton, MA).

2.3. Results

Based on the fitting of the Cs-137 clonogenic survival data, α_x and β_x values for both the H460 and H1437 cell lines were determined. These values are presented in **Table 4** and they have further been incorporated into calculations of RBE. Fitting of survival data for proton experiments produced α and β values for each of the 12 LET_d values at which measurements were performed. The ratios α/α_x and $\sqrt{\beta/\beta_x}$ (RBE_{max} and RBE_{min}, respectively) for each LET_d value are presented in **Figure 3**. Along with the ratios, the fitted curves of the data are presented, which constitute the RBE_{max} and RBE_{min} components of the proposed RBE model.

The equation for RBE_{max} is of the form

$$RBE_{max} = \frac{\alpha}{\alpha_x} = 0.75 + \frac{0.00143}{(\alpha/\beta)_x} LET_d^3 \quad (30)$$

where the scaling term for LET_d is inversely proportional to $(\alpha/\beta)_x$ and the function scales with the cube of LET_d. The function for RBE_{min} is of a similar form

$$RBE_{min} = \sqrt{\frac{\beta}{\beta_x}} = 1.24 + 0.00074 (\alpha/\beta)_x LET_d^3 \quad (31)$$

where the scaling term for LET_d is directly proportional to $(\alpha/\beta)_x$.

Figure 4 presents the comparison of seven RBE model predictions to the experimental RBE values for two experiments with H460 and two experiments with H1437. RBE is calculated at the 10% SF level. Most of the previously published models agree well with the experimental results up to an LET value of approximately 10 keV μm^{-1} . As a result of the fitting of the data, the new model provides a better prediction of the results beyond 10 keV μm^{-1} . The new model also displays an ability to account for the biological differences in the two cell lines due to its dependence on their photon biological parameters.

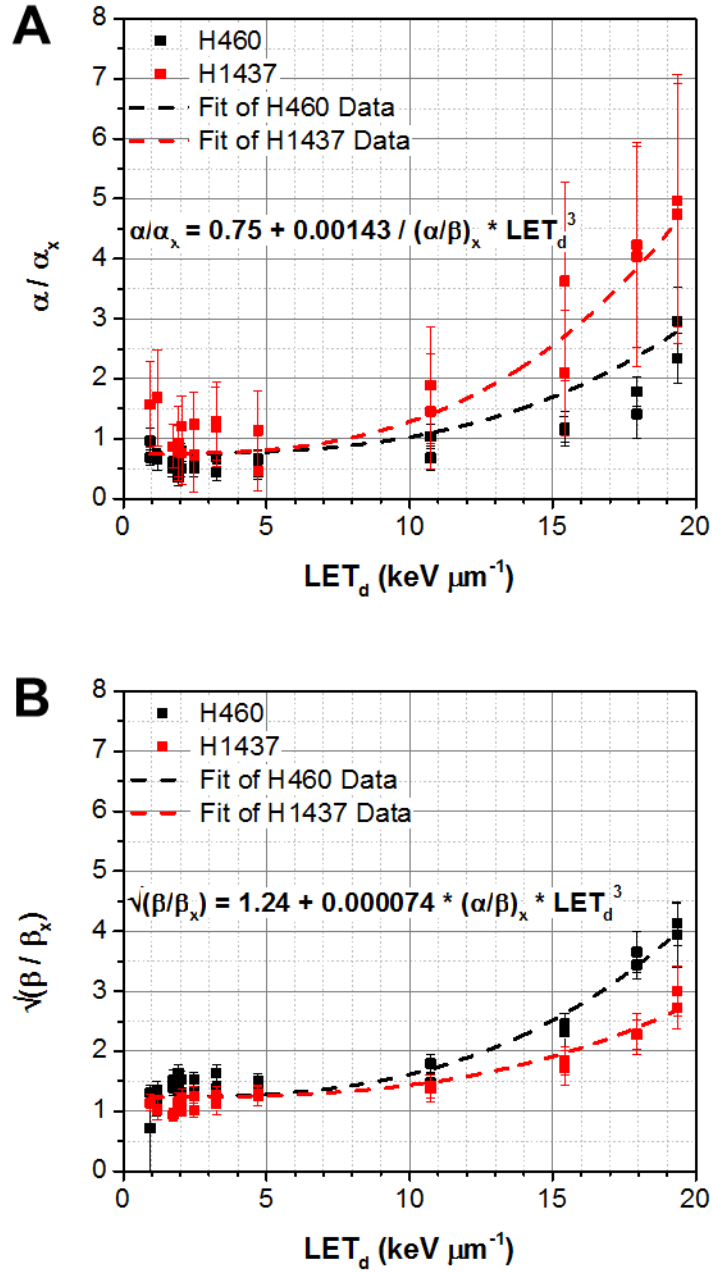


Figure 3: Fitting of the ratios α/α_x and $\sqrt{\beta/\beta_x}$ as functions of LET_d for both the H460 and H1437 cell line experimental results.

The ratios (A) α/α_x and (B) $\sqrt{\beta/\beta_x}$ are presented for the H460 (red dots) and H1437 (black dots) experimental data. Fits of the ratios as cubic functions of LET_d are also presented.

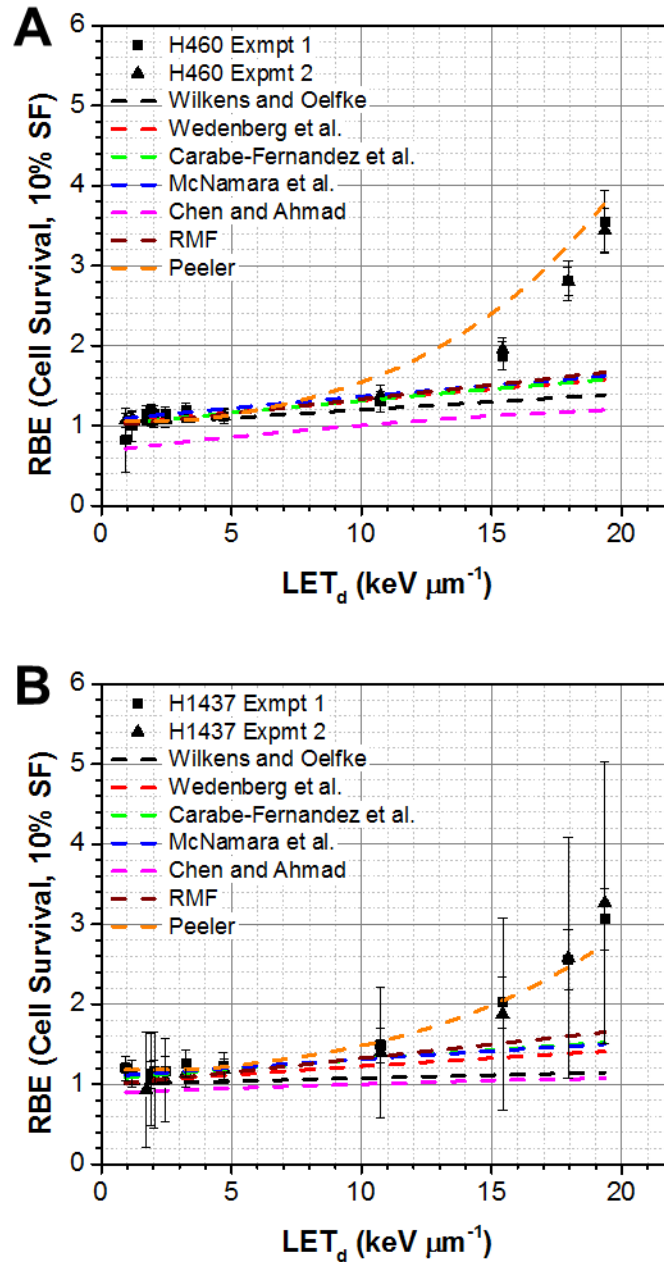


Figure 4: Comparison of measured and model calculated (including new model fit) RBE vs. LET_d for both the H460 and H1437 cell lines.

Predicted RBE values from seven models (Wilkens and Oelfke²², Wedenberg et al.²⁵, Carabe-Fernandez et al.^{27,28,31}, McNamara et al.³², Chen and Ahmad²⁶, RMF^{23,24,29,33}, and the new model from this work (Peeler)) are compared to the experimental results for both the (A) H460 and (B) H1437 cell lines.

2.4. Conclusions

Results from clonogenic survival experiments performed at MD Anderson and the predictions of seven RBE models, including a new model created specifically for this study, have been compared. While the non-linear nature of the relationship between RBE and increasing LET was unexpected, the inability of currently published models of variable proton RBE to adequately predict these results was to be expected after observation of the experimental results. All of the currently published models generally predict a linear increase of RBE with increasing LET_d. This relationship of course originates from the data upon which the various models were fit. In some cases datasets with very large spreads in observed RBE values were used for fitting with the assumption that a linear fit of the data was the most reasonable approach. For this particular set of data, obtained with pristine monoenergetic beams, repeat experiments with two cell lines have shown that a non-linear increase of RBE with LET is reproducible with great consistency.

There are many potential reasons for the observed results. One of the most probable explanations can be attributed to the design of this experiment compared to the experiments upon which the published RBE models are primarily based. Previous cell survival experiments have, for the most part, been performed with spread-out proton Bragg peaks. In the creation of an SOBP, the spectrum of LET values of protons at a given depth becomes more muddled and spread out. This could potentially lead to a decrease in the effectiveness of the proton radiation as the average LET value would now be a result of many LET values with differing effectiveness. In the MD Anderson experiment, it was shown that the spectrum of LET values represented by the average LET in each column of the well plate was actually quite narrow, at the very least more narrow than what would be observed in an SOBP¹⁹.

The overall conclusions to be drawn for this aim are that current RBE models may not be adequate for predicting experimental results for narrow LET spectra, particularly in the high LET region of the proton Bragg peak. A new model based on an empirical fit of the experimental results has been developed and will thus be carried through for analysis in patient treatment plans in Specific Aim 2 of this study.

Chapter 3: Comparison of RBE Models for Treatment Plans

3.1. Motivation

Specific Aim 2: To determine if there is a clinically significant difference between RBE-weighted proton treatment plan dose distributions calculated using different RBE models.

It has now been shown that published RBE models cannot adequately predict RBE for high LET_d as measured from high-resolution experiments. This is particularly the case for LET_d values above $10 \text{ keV } \mu\text{m}^{-1}$. While this is obviously relevant in the experimental setting, it is important to determine the relevance of such differences within the scope of patient treatment plans, which constitute different proton energy spectra and different values of LET_d . Toward this objective, the RBE models will be implemented in a system for calculating patient treatment plans.

One of the key components for calculating RBE is LET; however, the commercial treatment planning system (TPS) employed at MD Anderson does not have the capability to compute LET values for clinical treatment plans. This data is necessary in order to calculate RBE, so it must thus be obtained by some other method. The primary method employed for calculating accurate dose and LET for protons and other ions is known as the Monte Carlo method. This is a computing technique in which the interactions of single particles may be simulated from their creation until all of their energy has been deposited. This process is repeated hundreds, thousands, or millions of times until an average distribution of acceptable statistical accuracy is obtained. This method will be employed here for the purpose of obtaining dose and LET for the treatment plans of the cohort of interest that was previously identified in Section 1.6. The data will then be utilized to calculate RBE and RWD for seven RBE models. The results will then be compared to determine if any single model provides the greatest difference between constant

and variable RBE-weighted dose. The identified model will be carried forward for the analysis of outcomes for the patient cohort in Chapter 4.

3.2. Methodology

3.2.1. Treatment Plans of Interest

Thirty-four pediatric ependymoma patients treated with protons were selected for analysis in this study. These patients were treated as part of the prospective protocol of normal tissue toxicity with proton therapy that was examined in the study by Gunther et al.⁵⁸. All patients were treated with PSPT with the exception of one patient who received an IMPT boost plan. Patient treatments consisted of a primary plan and one or two boost plans. Dose prescriptions were between 54 and 59.4 Gy in 1.8 Gy fractions. In terms of treatment plan design, only the characteristics of the delivered dose are of interest for this analysis.

3.2.2. Computing Treatment Plans with MCNPX

For the purposes of this study, the Monte Carlo method is employed to calculate dose and the LET for treatment plans of interest. An in-house system known as MC², based on the Monte Carlo code MCNPX⁵⁹, is employed for this purpose. The system is designed to accept patient treatment plan information in a standard format called Digital Imaging and Communications in Medicine (DICOM). A C++ program reads this information and converts it into input files acceptable by the MCNPX program.

As an example, for PSPT treatment plans, this involves the creation of a digital model of the proton treatment delivery system, assigning the specific proton energies employed in the treatment plan, creating an MCNPX-compatible representation of the patient geometry (obtained from the patient's planning CT images), and specifying which data is to be collected

and in what region. For PSPT plans, a separate file is created for each energy of the proton beam used to create the SOBP. For each file, the MCNPX simulation is run for millions of particles. Once all of the simulations have been completed, the collected data is combined according to weighting factors assigned to each energy obtained from the DICOM plan file. Based on the specific components of the treatment delivery snout utilized in a particular treatment plan, the number of protons used for the simulations is converted into monitor units (MUs) and then scaled based on the actual number of MUs delivered to the patient. The MCNPX code is specifically used to obtain energy deposition data, which can be converted directly to dose, and the total proton fluence in each sub-volume, or voxel, of the patient treatment plan. This information can be used to calculate LET_t according to **Equation (1)**, since this operation is effectively the total dose divided by the total fluence.

While most studies have been based on LET_d , the LET_t is an acceptable approximation for LET_d for lower values of LET, such as those encountered in most patient treatment plans. LET_t has been shown to be linearly proportional to LET_d in this low LET region¹². Many of the patient treatment plans consisted of a primary plan and one to two boost plans. As such, the dose and LET values used are sum and average values, respectively, over all plans for a given patient.

3.2.3. Computing Variable RBE with MC data

The MC² system currently does not have any built-in functionality to perform RBE calculations based on the simulation output. This operation is thus performed using Matlab 2014b (The MathWorks, Inc., Natick, MA) due to its inherent advantages in working with matrix-based data. The seven RBE models employed in the analysis in Chapter 2 were also implemented in the Matlab treatment plan RBE calculation infrastructure. For the purpose of

Table 5: α_x and β_x parameters and ratios for normal tissues of interest.

LQ model parameters for the brain and brainstem obtained from Frese et al.³⁰ The endpoint of relevance for the presented tissues is necrosis/infarction.

Tissue	Endpoint	α_x (Gy ⁻¹)	β_x (Gy ⁻²)	$(\alpha/\beta)_x$ (Gy)
Brain/Temporal lobes	Necrosis/infarction	0.0620	0.0310	2
Brain stem	Necrosis/infarction	0.0532	0.0266	2

this study, RBE was calculated according to LET_t, which was in turn calculated as an average value over all treatment beams and plans for a given patient.

Because most of the models are empirical fits of measured data, their implementation was straightforward; however, for the RMF model, which is semi-mechanistic, additional data was needed for calculation. The MCDS^{24,40–43} software was used to obtain data for DSB Gy⁻¹ Gbp⁻¹ for a range of proton energies relevant to that which would be encountered in treatment plans. Using a reference value of 8.3 DSB Gy⁻¹ Gbp⁻¹ for Co-60 γ -rays, RBE_{DSB} was calculated for the spectrum of proton energies. The data was fit with a quadratic function resulting in **Equation (32)**.

$$RBE_{DSB} = 0.0011 * LET^2 + 0.0394 * LET + 0.9707 \quad (32)$$

Similarly, data for \bar{z}_F was also collected for the range of energies and fit with a linear function represented by **Equation (33)**.

$$\bar{z}_F = 0.0131 * LET + 0.0088 \quad (33)$$

These steps were necessary as these pieces of information could not be dose-averaged on a voxel-by-voxel basis because the full proton energy spectrum was not produced by MCNPX.

Normal tissue effects in the brain and brainstem are of particular interest for this study, so RBE was calculated based on these structures only. The biological parameters for photons for the brain and brainstem were obtained from a study by Frese et al.³⁰ **Table 5** displays the values for α_x , β_x , and $(\alpha/\beta)_x$ for both brain and brainstem that were utilized for RBE calculation. The value for the Wilkens and Oelfke²² model parameter λ used for RBE calculation was also taken from the study by Frese et al.³⁰ but rounded to be $0.01 \mu\text{m keV}^{-1} \text{Gy}^{-1}$.

3.2.4. Comparison of Constant and Variable RWD for Treatment Plans

For the previously identified patient cohort of interest, constant and variable RBE-weighted total plan doses were computed for all patients. Mean and max constant RBE-weighted dose, variable RBE and variable RBE-weighted dose, and LET_t for the clinical target volume (CTV), brain, and brainstem were computed. Difference between mean constant RBE-weighted dose and variable RBE-weighted dose for all RBE models for all patients was compared using a two-sided paired t-test of difference. Mean difference, standard deviation, and significance of the test are reported for all models.

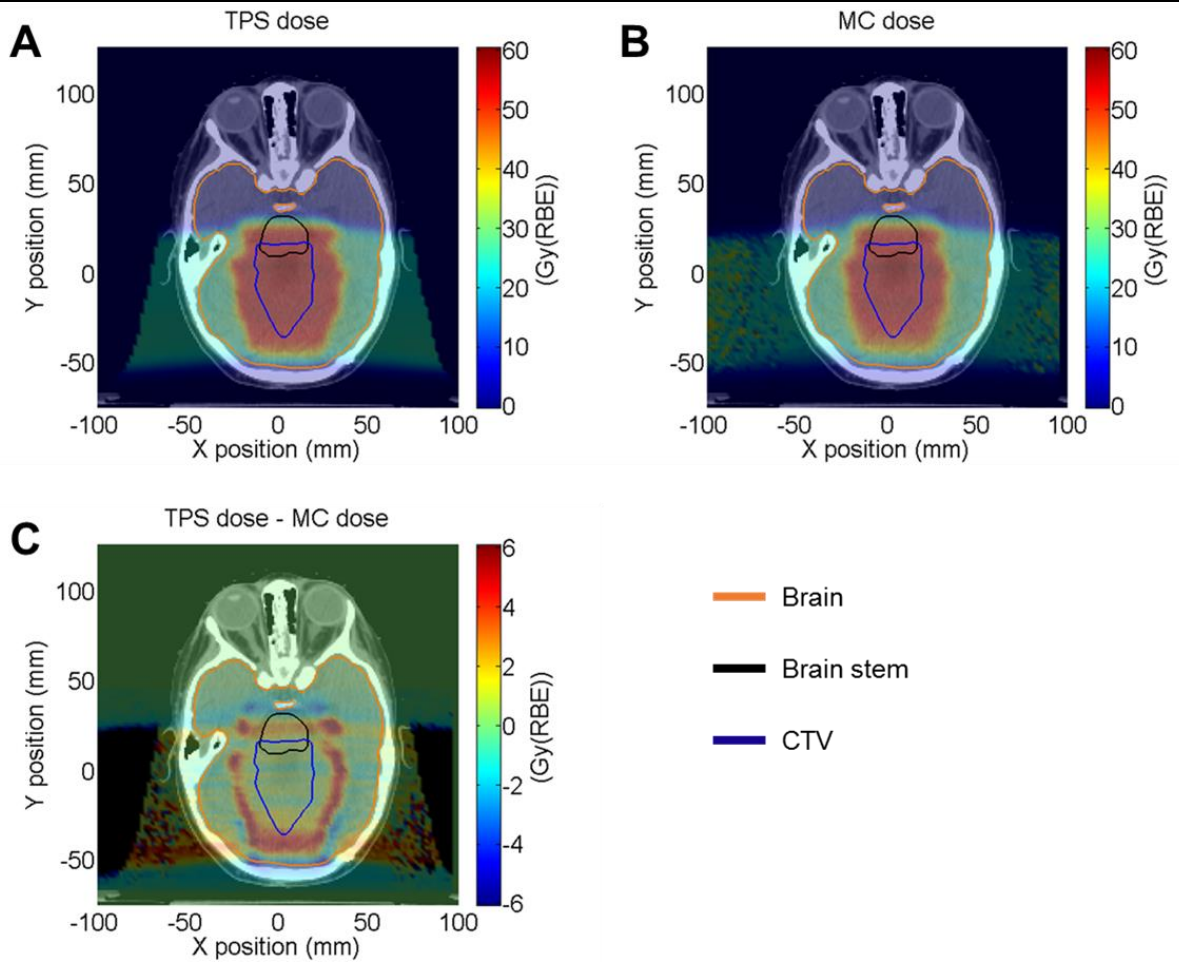


Figure 5: TPS and MC dose and dose differences for an example treatment plan.

Constant RWD from the (A) TPS and (B) MC simulations are presented. The difference between TPS and MC doses distributions (TPS dose - MC dose) is presented in panel (C). Structure contours for brain (orange), brain stem (black), and the CTV (blue) are included.

3.3. Results

Examples of TPS dose, MC dose, and their difference for a single patient are presented in **Figure 5A**, **Figure 5B**, and **Figure 5C**, respectively . For this example beams are impinging from the lateral directions and the greatest differences between the TPS and MC doses are in the regions near the lateral edges and end of range of the beams. Observed differences are on the order of approximately 5 Gy with the MC simulations predicting lower dose.

An additional example comparing MC calculated constant RWD and variable RWD calculated according to the McNamara et al.³² model is presented in **Figure 6**. The corresponding LET_t distribution is included in **Figure 6C**. As expected, the variable RWD is observed to be greater in the distal edge and distal falloff regions of the beams, which is represented in **Figure 6D**.

The results of the collected analysis of the differences between variable and constant RBE-weighted dose are presented in **Table 6**. Despite the small number of patients analyzed (34 in total), all of the models are observed to produce significantly different mean CTV doses according to a two-sided paired difference test. The model by Chen and Ahmad provides the greatest differences; however, the difference is so great that it may likely be attributed to improper scaling of the model for different cell lines. The model displaying the next greatest difference is that by McNamara et al.³² which shows a 7.2% increase in variable RBE-weighted dose over constant RBE-weighted dose.

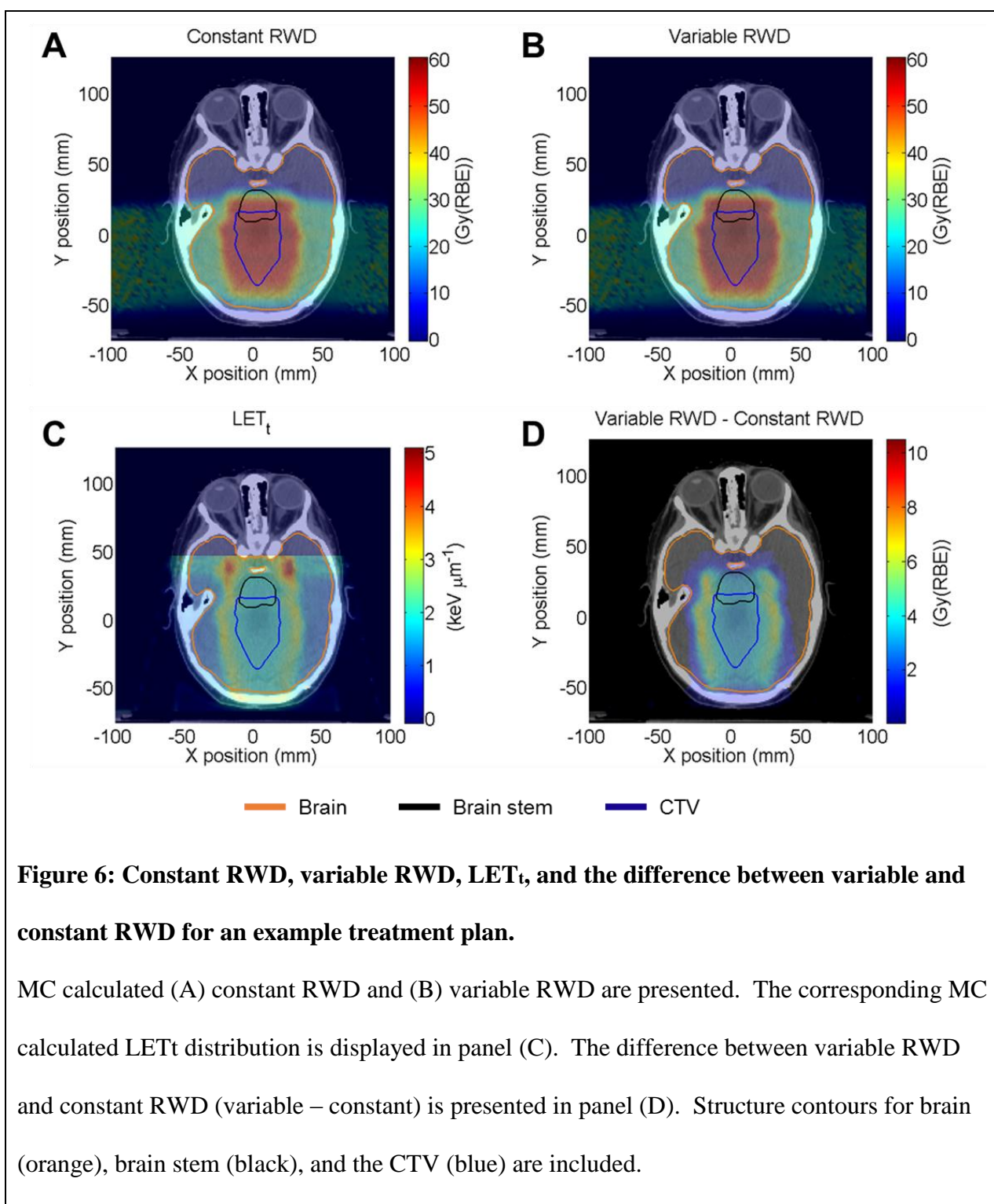


Figure 6: Constant RWD, variable RWD, LET_t , and the difference between variable and constant RWD for an example treatment plan.

MC calculated (A) constant RWD and (B) variable RWD are presented. The corresponding MC calculated LET_t distribution is displayed in panel (C). The difference between variable RWD and constant RWD (variable – constant) is presented in panel (D). Structure contours for brain (orange), brain stem (black), and the CTV (blue) are included.

Table 6: Comparisons of Mean CTV variable and constant RWD for multiple RBE models.

The differences between mean variable RWD and constant RWD in the CTV over 34 patients for seven RBE models are presented. The models include those by Wilkens and Oelfke²², Wedenberg et al.²⁵, Carabe-Fernandez et al.^{27,28,31}, McNamara et al.³², and Chen and Ahmad²⁶, as well as the RMF^{23,24,29,33} model and the model developed for this work (Peeler). A two-sided paired difference test was performed to determine significance. P values were evaluated at the 0.05 significance level. Mean differences as a percent of the mean constant RWD are also included.

RBE Model	Mean Difference: Variable - Constant RBE Dose(Gy)	StDev	P-value (Null: Mean = 0)	Difference as % of Constant RBE Dose
Wilkens and Oelfke	-1.2	0.8	6.7E-05	2.1
Wedenberg et al.	1.9	0.9	1.7E-06	3.3
Carabe-Fernandez et al.	2.0	0.8	5.2E-07	3.6
McNamara et al.	4.1	0.7	1.4E-11	7.2
Chen and Ahmad	20.3	2.9	1.4E-12	35.8
RMF	-2.3	0.6	1.5E-09	4.0
Peeler	-2.3	0.2	2.3E-16	4.0

3.4. Conclusions

Comparison of constant RWD between the TPS and MC system revealed that the systems do have differences in their calculations of proton dose distributions evidenced by lower MC calculated dose in the distal and lateral edges of the proton beams compared to the TPS. This is observable in **Figure 5C**. These differences can be sourced to a number of factors arising from the inherent differences between TPS and MC dose calculation. The TPS calculates dose by converting pre-measured or pre-calculated proton depth dose distributions into an analytical

function which is then used to calculate dose on the patient geometry. This method cannot fully account for energy straggling and lateral scattering effects which are modeled in the MC physics calculations^{60,61}. These effects can lead to lower MC calculated dose in the distal and lateral edges^{62,63}. It has been observed that this degradation of the distal edge of proton beams is often not adequately modeled by the TPS dose calculations, particularly in heterogeneous materials^{62,64–66}. TPS analytical algorithms have also been shown to approximate the way in which the proton beam shines on the range modulator in PSPT, resulting in overestimation of the dose on the proximal edge of the SOBP⁶⁷, which can result in a further reduction in dose when the proximal edge of a beam overlaps with the distal edge of another beam.. Additionally, the methods by which the two systems account for material densities are different. The TPS determines electron density directly through CT numbers from the planning CT, while for the MC simulation the planning CT is converted into specific material specifications in the input file. Differences in material density between the two systems could lead to differences in calculated dose. In general, the differences between the systems were on the order of 5 Gy and, importantly, were not observed in the region of the CTV, which was used for analysis here.

This specific aim has resulted in the capability for calculating variable RWDs for seven RBE models based on the output data of the MC² system. Analysis of the results for a cohort of patients has shown that differences in mean values for variable RWD compared to constant RWD in the CTV structure are significant for all of the analyzed RBE models. In particular the models by Wedenberg et al.²⁵, Carabe-Fernandez et al.^{27,28,31}, and McNamara et al.³², and Chen and Ahmad²⁶ provide increases over the constant RWD, while the model by Wilkens and Oelfke²², my own model, and the RMF model^{23,24,29,33} show decreases in mean CTV dose. The results produced by the model from Chen and Ahmad²⁶ appear to be outlier values, but this is to be somewhat expected since the model was fit for specific cell line with no inherent scaling

mechanism for different cell lines. Of the models providing an increased variable RWD compared to constant RWD, the model by McNamara et al.³² exhibits the greatest difference that would not be attributed to potentially erroneous values (i.e. the Chen and Ahmad model²⁶). The McNamara et al.³² model will thus be carried forward for the analysis performed in Specific Aim 3.

Chapter 4: Assessing the Role of Variable Proton Biological Effectiveness in Observed Treatment Outcomes

4.1. Motivation

Specific Aim 3: To determine if the spatial location of proton radiation induced imaging changes is associated with the variable biological effectiveness of proton radiotherapy.

While laboratory studies suggest increased biological effectiveness near the end of proton beams, to date there is little evidence to suggest that such changes are important clinically. Initial studies have looked for clinical evidence of increased biologic effectiveness with mixed results²⁰. This may be in part due to the fact that such studies have looked to map proton RBE as a function of dose and LET (and sometimes other factors) using models based on in vitro experiments performed with various cancer cell lines^{11,19,20,32,68}. Such models, typically involving measures of clonogenic survival, may not be applicable to complex in vivo processes including multiple cell types, such as radiation-induced brain damage. The apparent lack of evidence may also be due to multiple other sources of uncertainties that may obscure consequences of approximation in RBE.

In the realm of photon therapy, the appropriate safe and effective doses for treating various types of tumors and the tolerance doses for normal tissues have been derived from the collected analysis of decades of patient outcomes data^{50,69–71}. When assessing a newer technology such as proton therapy, it would make sense to take a similar approach to develop such knowledge. However, because of the limited availability of proton therapy, patient data is limited; yet given its high cost, there is pressure to fully elucidate the benefit of proton therapy^{72–74}.

Gunther et al. recently identified that, in comparison to patients treated with photon therapy, children with ependymoma treated with protons more frequently developed post treatment MR imaging changes in normal brain parenchyma⁵⁸. Such changes in imaging biomarkers are considered a grade 1 toxicity and although many patients will not develop clinical symptoms, such imaging changes are important for studying the biological properties of protons as a function of dose and LET. While clinical factors, such as age, may account for some difference, this study seeks to analyze patients treated with protons to determine if the location of post-treatment image changes are related to physical proton characteristics, more specifically LET. By looking at voxel-level data rather than only volume-based data, this study seeks to improve the ability to correlate clinical imaging data with dose and LET.

4.2. Methodology

4.2.1. Patient Cohort and Image Processing

The same 34 pediatric ependymoma patients treated with protons from the Gunter et al. study are again analyzed here. A subset of 14 patients exhibited post-treatment MR imaging changes observable as T2-FLAIR hyperintensity with or without enhancement on T1 post-contrast sequences. MR images were rigidly registered with treatment planning CT images using the Eclipse treatment planning system (TPS) v9.0 (Varian Medical Systems, Inc., Palo Alto, CA). Regions of treatment-related change in normal brain parenchyma were contoured by a practicing radiation oncologist based on the earliest post-treatment scan in which image changes were observed.

4.2.2. Voxel-level Analysis of Image Changes

In order to prevent fracturing and reducing the size of the data set, all image changes were evaluated as being within the whole brain. The contoured image change regions were identified with voxels represented as binary response (image change) 1 while voxels within the brain outside of the response region were represented as response 0. Combined with the dose and LET_t data, this produced over eight million ‘events,’ each with its corresponding dose, LET, and image change status (0 or 1). Voxel data points with dose below 1 Gy were then removed from the dataset because these points were effectively noise and no image change would be expected to be observed at this dose. Using the Matlab 2014b *glmfit* function, a generalized linear model fit of the data was performed according to the binomial distribution with a probit link function. Dose and LET were taken to be the predictors in the model. The probit model assumed in the fitting is the normalized cumulative distribution function with $\mu = 0$ and the standard deviation $\sigma = 1$, which results in the same general probit model utilized by Lyman for NTCP calculation represented by **Equation (26)**⁴⁸. In this case P is the probability of image change. The result of the fitting is a set of coefficients for a linear function of dose and LET, which is represented by the variable c in **Equation (26)**.

4.2.3. Statistical Analysis

A set of 10 clinical and treatment factors were selected for logistic regression analysis to determine if there was any association with the presence of image changes. Of the clinical factors analyzed in the paper by Gunther et al., age at radiotherapy and time before radiotherapy (after surgery) were selected for inclusion in this analysis due to their trends toward significance in that study⁵⁸. The other eight factors selected for this study include mean and maximum LET, mean and maximum physical dose, mean and maximum variable RBE, and mean and maximum

variable RBE-weighted dose in the CTV. RBE values were calculated using the model by McNamara et al.³² Univariate and multivariate logistic regression analysis was performed using Matlab 2014b in order to determine if any were significantly associated with the presence of image changes. Odds ratios and 95% confidence intervals (CI) were calculated for each factor. Factors with p value less than 0.25 on univariate analysis were included in the multivariate analysis. No interaction variables were included in the multivariate analysis.

Leave-one-out cross validation (LOOCV) was performed in order to test the robustness of the fitted generalized linear model. For this dataset, which consists of a very large number of voxels, traditional LOOCV would not provide a reasonable assessment of the model. The cross validation was performed by successively leaving out all of the voxels from each individual patient with image changes and then testing the model on the left out set of voxels. The data from the patients without image changes was included in each of the training datasets and effectively served as additional control data for no image change. Model parameters were calculated for each of the 14 left-out patients. For each iteration, a receiver operating characteristic (ROC) curve was produced and the area under the curve (AUC) was calculated using the Matlab *perfcurve* function. This could not be performed for the patients without changes because there would be no true positive cases in the test dataset. This is yet another reason why this data was simply included in all of the training datasets.

Table 7: Univariate and multivariate logistic regression analysis on clinical factors for all patients.

Results of univariate logistic regression analysis are presented for 10 clinical and treatment factors for the 34 patients of interest. Binary classifiers were determined based on mean values over all patients. Four factors with p-value < 0.25 on univariate analysis were also included in multivariate logistic regression analysis.

Variable	Odds Ratio	95% CI	P Value - Univariate	P Value - Multivariate
Mean LET in CTV				
> 1.5 keV μm^{-1}	8.67	0.94 - 80.0	0.06	0.63
Max LET in CTV				
> 2.5 keV μm^{-1}	7.33	1.29 - 41.7	0.02	0.53
Mean CTV physical dose				
> 52 Gy	0.61	0.15 - 2.43	0.49	
Max CTV physical dose				
> 56 Gy	0.82	0.21 - 3.22	0.77	
Mean CTV RBE				
> 1.16	0.44	0.10 - 1.92	0.28	
Max CTV RBE				
> 1.22	0.92	0.23 - 3.63	0.90	
Mean CTV RWD				
> 61 Gy(RBE)	0.50	0.13 - 2.00	0.33	
Max CTV RWD				
> 65 Gy(RBE)	1.00	0.26 - 3.92	1.00	
Age at RT				
< 3 years	2.50	0.58 - 10.7	0.22	0.65
Time before RT				
< 3 Months	7.00	0.75 - 65.2	0.09	0.30

New abbreviations: RT = radiotherapy

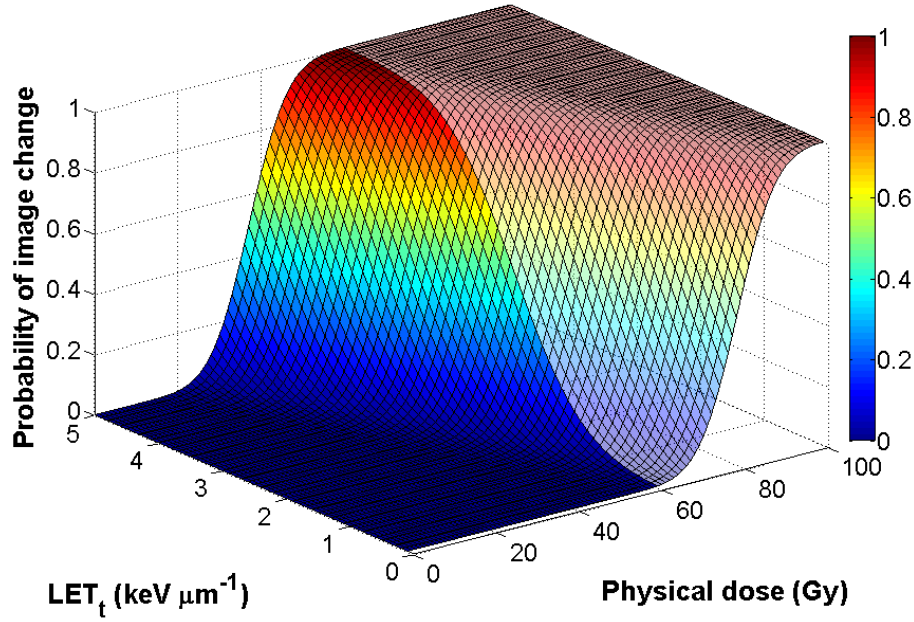


Figure 7: Surface plot of generalized linear model for image change based on dose and LET_t .

Three-dimensional representation of the fitted generalized linear model that predicts probability of image change in a voxel as a function of dose and LET_t . The faded portion of the surface indicates the region above the maximum physical dose observed in the patient cohort (60 Gy). This region is extrapolated from the model. The maximum LET_t observed within the image change regions was $5 \text{ keV } \mu\text{m}^{-1}$, thus the LET_t axis is not further extrapolated in the figure.

4.3. Results

A total of 10 clinical and treatment factors, which are presented in **Table 7**, were analyzed to determine any association with the presence of image changes. Of the factors presented, only maximum LET_t in the CTV was found to be significant ($p = 0.02$) at the 0.05 level on univariate logistic regression analysis. Mean LET in the CTV ($p = 0.06$), age at radiotherapy ($p = 0.22$), and time before radiotherapy ($p = 0.09$) all presented $p < 0.25$ and were thus included in multivariate logistic regression analysis. None of the factors were subsequently found to be significant at the 0.05 level on multivariate analysis.

Figure 7 presents the results of fitting a generalized linear model for image change based on the dose and LET predictors. The model was evaluated for a distribution of dose and LET values to produce the surface plot. The faded region in **Figure 7** indicates values that are extrapolated beyond the data used for the fitting of the model. The reported model parameters are the result of cross-validation performed by fitting the model while successively leaving out each of the patients with image changes. The generalized linear model is represented by the following equation

$$c = 1.2 * LET_t + 0.14 * Dose - 11.2 \quad (34)$$

in which the coefficients are the mean values determined through cross validation. The standard deviations of the LET_t coefficient, dose coefficient, and intercept are 0.1, 0.01, and 0.7 respectively.

In order to better visualize the relationship between image change, dose, and LET_t for different values of dose and LET_t, **Figure 8A** and **Figure 8B** display two-dimensional slices through the surface for constant LET_t of 1, 2, 3, 4, and 5 keV μm^{-1} and constant physical dose of 30, 40, 50, 60, and 70 Gy, respectively. It is further possible to extract more traditional values

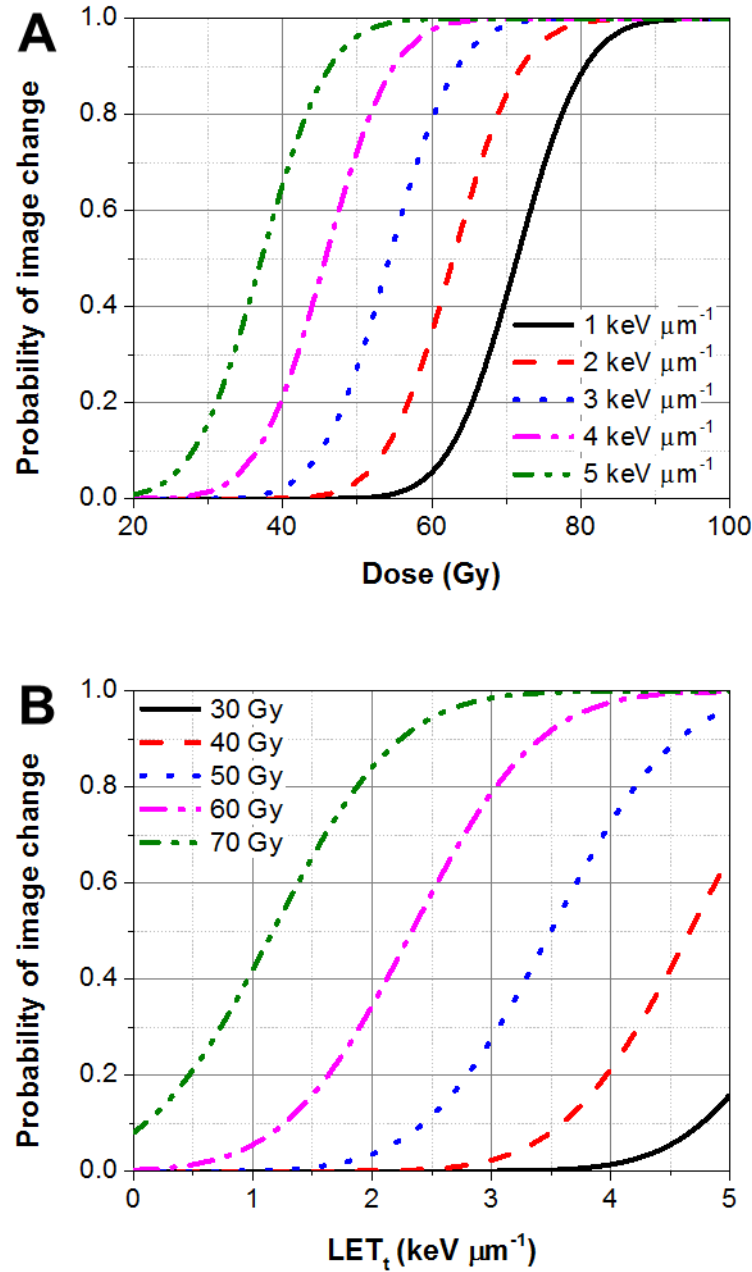


Figure 8: 2-D representations of the generalized linear model for image change for constant LET_t or physical dose.

Curves represent slices through the 3-D surface produced by the generalized linear model for (A) constant LET_t of 1, 2, 3, 4, and 5 keV μm⁻¹ and (B) constant physical dose of 30, 40, 50, 60, and 70 Gy.

for TD_{50} , the tolerance dose at which a toxicity would be expected to be observed in 50% of patients, for different values of proton LET_t . This data is presented in **Figure 9**. The TD_{50} data were fit with a linear equation (the expected result due to the generalized linear model fitting) which is represented by **Equation (35)**.

$$TD_{50} = 80.0 - 8.57 * LET_t \quad (35)$$

TD_{50} is observed to decrease with LET_t , a trend which indicates an increase in biological effectiveness of proton dose with increasing LET_t consistent with traditional RBE models for proton therapy.

A more practical representation of the model is presented in **Figure 10**. Dose and LET distributions for an example patient are plotted on an axial CT slice in **Figure 10A** and **Figure 10B**, respectively. The LET distribution in the figure has an abrupt edge due to the size of the grid used for Monte Carlo calculations. Dose and LET beyond this edge were not calculated because the region is out-of-field and limiting the size of the calculation grid allows for improved calculation efficiency. The probability of image change is plotted in **Figure 10C**. Qualitatively the areas of increased probability of image change predicted by the model are observed to overlap with the region of image change indicated by the contour generated using the registered post-treatment MR image.

Cross validation of the model generated 14 ROC curves, one for each leave-out iteration. The cross-validated AUC for the model was 0.91 with a 95% confidence interval (CI) of 0.88 – 0.94.

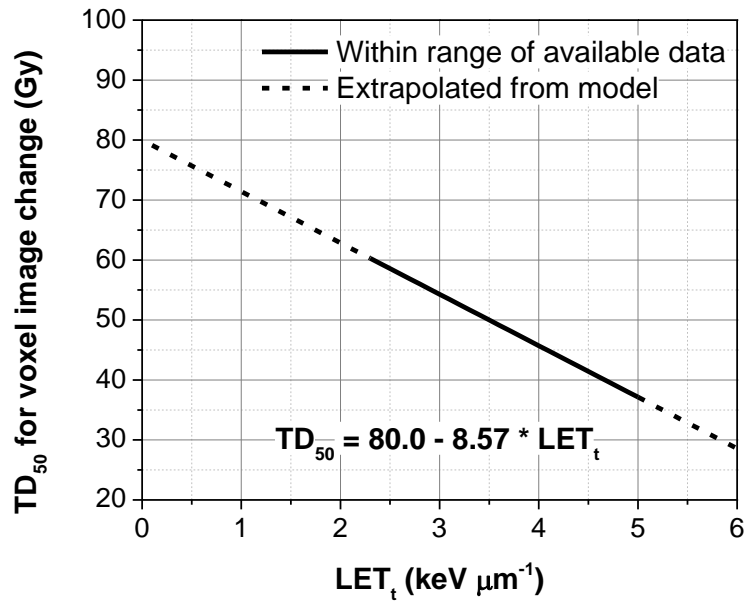


Figure 9: TD_{50} as a function of LET_t based on interpolation of the generalized linear model for image change.

Line displays the values for TD_{50} interpolated from the fitted generalized linear model for a range of LET values. The solid portion of the line represents the range of data observed in the patient cohort, while the dashed line represents extrapolation from the generalized linear model. The equation for a linear fit of TD_{50} versus LET is also presented.

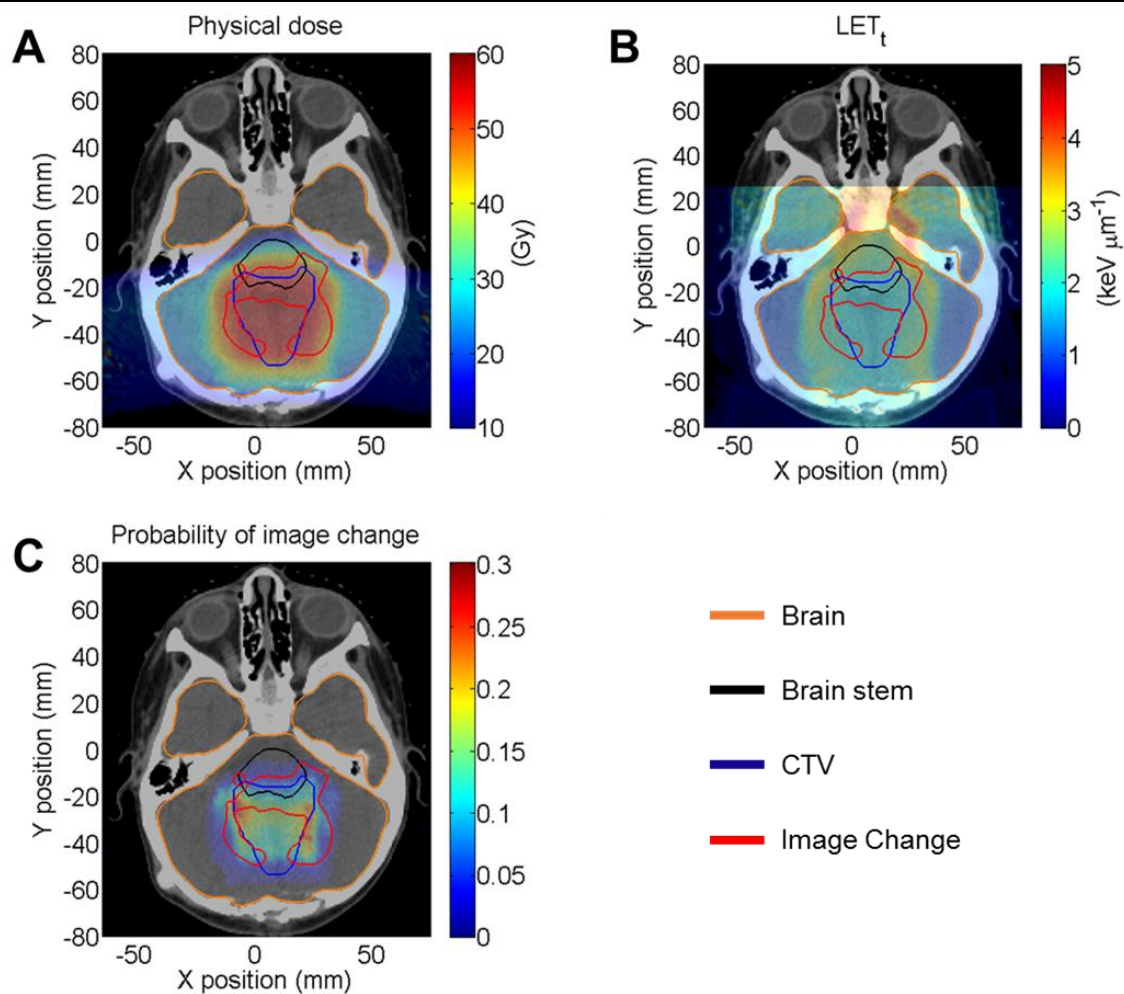


Figure 10: Dose, LET_t , and probability of image change distributions for an example patient.

Figure displays (A) physical dose and (B) LET_t distributions on an axial CT slice for an example patient. Probability of image change calculated with the generalized linear model is presented in panel (C). Structure contours include the image change region (red), brain (orange), brain stem (black), and CTV (blue).

4.4. Conclusions

As in the Gunther et al.⁵⁸ study, the clinical factors age at radiotherapy and time before radiotherapy were found to trend toward significance on univariate analysis in this study; however, they were found to not be significant on multivariate analysis. Unfortunately, these clinical factors cannot be overcome by the use of the voxel-level analysis since they are patient specific and thus modeling their impact is very much beholden to the number of patients in the study. Simply including them as predictors in the generalized linear model is not viewed as an adequate consideration of their effect because there is no evidence to suggest that they would be best modeled linearly, unlike LET effects. Analysis of more patient data may eventually allow for development of different models for different ranges of ages at treatment and time between surgery and radiation therapy.

Interestingly, the selected treatment factors related to dose and LET were not found to be significant on multivariate analysis. This is not necessarily unexpected because the entire purpose of carrying out voxel-based data analysis was to overcome some of the inherent problems of point and volume-based analysis. In this sense, given the results, the image changes observed can more likely be attributed to dose and LET distributions in certain sub-volumes of tissue, which would be difficult to observe through whole organ volume or point based measures.

This analysis has shown that voxel-based, post-treatment MR image changes in pediatric patients treated with proton therapy are dependent on both physical dose and LET_t. A generalized linear model based on a probit link function was developed which can describe the decrease in the TD₅₀ for image change as proton LET increases. The ROC curves describing the model's ability to positively identify voxels with image change had a cross-validated AUC of 0.91 (95% CI: 0.88-0.94). To my knowledge, this is the first example of the extraction of

proton biological effectiveness information from clinical data. The success of this study supports the continued investigation of proton therapy outcomes with the goal of identifying other quantifiable responses or toxicities that could be used to further the collective understanding of proton biological effectiveness in humans. Models developed from this type of analysis could eventually be used prospectively to design safer and more effective proton treatments.

Chapter 5: General Discussion

5.1. Summary and Discussion of Findings

The central hypothesis of this work was that radiation-induced image changes observable on follow-up imaging could be attributed to the variable biological effectiveness of proton radiotherapy. The approach taken to test this hypothesis first involved the identification of appropriate models for calculating the variable RBE of protons. New high-resolution cell survival data produced by the MD Anderson proton therapy research group was utilized here for the purpose of testing the accuracy of the models on a more robust data set than those used for the creation of the models. Comparison of the model output to the experimental data proved that the models cannot adequately reproduce the RBE for high LET protons measured from the experiments. The models and experiments typically began to deviate in the region where LET was greater than $10 \text{ keV } \mu\text{m}^{-1}$, which corresponds to the region of the proton Bragg peak and distal falloff. A new model was fit based on the experimental results from the two analyzed cell lines, with consideration to the incorporation of the photon $(\alpha/\beta)_x$ into the formalisms for RBE_{\min} and RBE_{\max} such that the resulting model might be more translatable to other experimental cell lines employed in the future.

All of the selected RBE models and additionally the newly developed model were then implemented into a codified form that could be used to calculate RBE for patient treatment plans based on the output of Monte Carlo simulations. Monte Carlo simulations were performed for a group of 34 patients treated on protocol with PSPT who were of interest due to their high rate of occurrence of post-treatment image changes observed on MRI. For this step of the study, the variable RBE-weighted dose distributions from all models for all of the patients were compared in order to determine if any particular model could prove more useful in determining if the location of the image changes was related to RBE. As a result of this

analysis, the RBE model by McNamara et al.³² was identified to produce the greatest positive difference, on average, between variable and constant RWD. This comparison was performed for the CTV structure in particular due to the fact that many of the identified image changes occurred in-field. While the model by Chen and Ahmad²⁶ did actually produce the greatest difference in doses, it was decided that the predicted differences were unreasonably large, most likely due to the model's lack of inherent scaling with the reference radiation alpha/beta ratio for a particular cell type.

Comparison of average volumetric variable RWD values between patients presenting with image changes and those without showed no significant differences between the two groups. This result motivated a shift in approach such that voxel-based data would be analyzed instead of volumetric data. Based on the probit dose-response relationship, which is traditional to radiation therapy outcomes analysis, a generalized linear model was fit according to all of the voxel-based data from the 34 patients of interest. Using the image change data to define a binary response metric, the probability of response based on the developed model was observed to increase with LET_t for a given physical proton dose. Statistical analysis of the model output was performed through LOOCV. The average AUC over the ROC curves calculated for each patient with image change was 0.91 (95% CI: 0.88-0.94) which is a high value, indicating that the model was robust for this data set and is more likely to be applicable to patients beyond this data set.

Variable proton biological effectiveness is not currently incorporated into clinical treatment planning. This is due in large part to uncertainty in published RBE values and the apparent lack of clinical evidence that the use of a constant RBE value leads to suboptimal outcomes²⁰. This study aimed to tackle the latter point by providing evidence that post-treatment changes observed on follow-up imaging studies are associated not only with dose but also with LET. In

pediatric ependymoma patients treated with proton therapy, I found significant correlations between spatial areas of image change and increasing LET.

The analysis presented was made with a novel method, which incorporates voxel-level data to correlate imaging change with physical dose and LET data from the treatment plan. This is a departure from the typical strategy of using whole organ volume-based data. I believe that my strategy is logical due to the nature of the response I am analyzing, i.e. to deduce the biological effect from the image change (image biomarkers). Image biomarkers are more likely to detect subtle changes due to differences in RBE that may be difficult to detect clinically. While image changes do not always lead to permanent adverse neurological defects^{58,75–77}, they are still considered to be at least a grade 1 response according to the Common Terminology Criteria for Adverse Events (CTCAE) v4.0⁷⁸ grading scale and may be a harbinger of more severe reactions^{79,80}. It is also worth noting that sample size requirements for image biomarker-based analysis is likely to be smaller than the traditional approach of correlating dose-volume indices with toxicities⁸¹. Being able to predict and potentially prevent post-treatment central nervous system (CNS) image change would ultimately improve treatment designs and, therefore, outcomes. The methodologies developed may also be applicable to other patient datasets and disease sites.

Previous studies have focused on applying pre-existing models of variable proton RBE for the analysis of patient cases^{82,83}. To date no significant correlations between increased RBE and observable treatment responses have been found. I have specifically avoided the use of existing RBE models in the final analysis of image changes so as to not constrain the results of the analysis to a pre-determined model. Such models have largely been developed from in vitro data, and there is no certainty that in vivo response would follow the same pattern.

The probit form of the model was chosen primarily because many previous dose response studies in radiation oncology have used the Lyman NTCP computation model, which is a probit model⁴⁸. As the published Lyman model does not have an LET component, it was not appropriate for use here in its standard form. I was, however, able to extract the TD₅₀ parameter since my model is based on the probit function. This allows one to relate the results back to the more traditional models and analyses. Published values for TD₅₀ of necrosis/infarction in the brain (the most closely related normal tissue effect for which there is a large collection of reported data) for photons are in the range of 60-75 Gy^{48,50,84,85}. My analysis indicates that, for this set of patients, the TD₅₀ for voxel image change spans a similar range for typical low proton LET values of 0-2 keV μm^{-1} . Such low LET values are common in the entrance region and portions of the target volume and have a similar biological effect as photons²⁰. Lower LET values correspond to higher TD₅₀ values which translates to decreased biological effectiveness. Finally, higher LET protons correspond to lower TD₅₀ values, which in turn corresponds to greater biological effectiveness. Here these LET values are in line with those near the end of the range of protons. Assuming a TD₅₀ of 65 Gy for brain necrosis for photons, the ratio of the photon values to that of protons eventually exceeds 1.1, which is the currently assumed value for proton RBE for clinical purposes. It should be noted that to my knowledge there is no definitive TD₅₀ for image changes reported for photon radiotherapy, yet these changes do represent early tissue damage.

Cross validation of the model by leaving out sets of data from individual patients indicated that the model could still perform well for each patient without their data being incorporated into the parameter fitting. The high value of the cross-validated AUC is viewed as a good indication that that model could be applied to patients outside of this cohort and still achieve favorable results. It should be noted, however, that the intended purpose of the model is

not to specifically identify voxels that will exhibit image change, but rather to provide a value for risk of change that can be used to optimize a plan in such a way as to reduce this risk.

5.2. Limitations

There are a number of limitations associated with this study that should be stated. One prevalent limitation is that LET_t is used for the treatment plan and outcomes analysis as opposed to LET_d . This is due to the fact that the MCNPX code used could not reasonably produce LET_d data for the patient geometries involved in the study. I would argue, though, that the impact of the use of LET_t is negligible because the LET values observed for the treatment plans were generally low, and in this region of LET values, LET_t and LET_d are nearly equivalent¹². Nonetheless, this issue could be overcome in the future by using a more efficient Monte Carlo code that could produce LET_d data.

Another issue related to LET is that an average LET value was employed for the voxel-based analysis. With more advanced Monte Carlo simulations, it would be possible to record information about the spectrum of LET values encountered in each voxel. In particular, this could help identify areas in which some proportion of the individual proton LET values are higher and thus produce more biological damage. Analyzing this data could provide a better realization of the effect of proton LET as it relates to the observed outcomes.

With the respect to the image data utilized in the study, a simplistic approach was taken. MR images were rigidly registered to treatment planning CT images. This method could fail to capture more subtle changes in the location of the soft tissue and thus affect the spatial relationship between the dose and the image changes. This could be overcome through the utilization of deformable image registration, which uses a greater number of anatomical landmarks to non-uniformly deform the MR images to the CT images.

One of the potentially more difficult limitations to address is the assumption that the response of individual voxels is independent from other voxels. The data represents a biological system in which the response of a subunit of tissue is affected by the response and changes in adjacent tissue. It was accepted that, as a first approach, assuming voxel independence was reasonable due to the lack of a better model. The exact initiating cause of the observed image changes is still poorly understood. The causes of symptomatic brain tissue damage are currently thought to be attributable to changes in vasculature or direct damage to supporting glial cells, or likely some combination of both of these effects⁸⁶⁻⁹⁰. Future research could eventually identify these mechanisms, which could potentially be incorporated to define better outcome models.

5.3. Significance and Future Directions

To date the vast majority of studies investigating the biological effects of protons have been focused on *in vitro* cellular response to different proton dose and LET^{11,19,20}. A large volume of data has been collected, but the published values for proton RBE continue to have large uncertainties due to many factors. Examples of such confounding factors include differences in dose and, in particular, LET calculation methods, differences in cell survival experiment methodology, inadequate reporting of experimental design and Monte Carlo calculation details, which can preclude reproduction of studies, and differences in data fitting methods. These factors can lead to differences between experimental data and models if the models were fit based on previous experiments. This study has shown that high-throughput and consistently reproducible radiobiological experiments may provide a more clear picture of proton RBE, including a nonlinear relationship between RBE and LET, which would be difficult to observe in the collected data from multiple institutions. This only further serves to highlight that proton RBE is an inherently uncertain quantity, and it will likely remain this way for some time.

Part of the analysis in this study was thus conducted with the goal of shifting the dialog away from RBE and instead toward the understanding of outcomes simply based on the physical properties of protons -- dose and LET. An advantage of this approach is that it provides the opportunity to become directly knowledgeable of the proton biological effects that are of greatest interest, i.e. those tied to observable clinical outcomes. As previously stated, this approach is limited due to lack of sufficient outcomes data in many cases. It can also be difficult to draw substantial conclusions from patient cohorts for which the size of the observed effect is small. This was likely the case for a similar study by Giantsoudi et al.⁸² which analyzed treatment outcomes for a cohort of patients treated for medulloblastoma. In a cohort of 111 patients, only 4 were observed to have symptomatic normal tissue complications. The study may have further been limited by analyzing patient data based on volumetric indices.

Previous models for normal tissue complications have been based on dose-volumetric data^{48,49,51}. While this methodology has been well studied, it may not be the most effective approach for analyzing proton therapy outcomes. Dose-volume indices represent averages over volumes and can thus hide positional information. While photon therapy has a reasonably constant LET value, proton therapy has an inherently spatially variant LET value. Thus, volume averaging of proton plan indices such as LET or values linked to LET, such as variable RWD, may wash out valuable information about focal areas of interest. DVH metrics do provide some value in observing these effects, but given the amount of computational power now available, it only makes sense to consider analyzing data on a voxel-by-voxel basis, especially considering that imaging technology can now provide a wealth of functional information at the voxel level. This study has provided strong evidence that such an approach can potentially enhance the value of the limited number of proton outcome studies currently available because it utilizes a greater amount of data from each patient.

In the current study, all patients were treated with passive scattering proton therapy. This is a traditional technique that allows little flexibility, similar to photon based 3D conformal radiation therapy. As with photon treatments, which have evolved to IMRT, pencil beam scanning technology is now allowing additional flexibility in proton planning and delivery with IMPT. This technology provides greater capability for advanced optimization techniques based on the simultaneous optimization of multiple treatment beams based on the placement of individual beamlets. This is important to highlight because the results of this study would be difficult to implement in PSPT treatment planning due to the limitations on plan optimization.

The development of proton biological effectiveness models is typically done with the intention of applying the model to evaluate the potential outcome of a given plan and to optimize plans to achieve better outcomes. The case is no different here. Using IMPT, the probability of image change provided by my model could be used in treatment plan evaluation and optimization, and in fact, this is included in my own plans for future research. I foresee being able to implement the model for probability of image change in a voxel into proton plan optimization as a constraint in the objective function. A goal for the optimization could then be to keep the probability of image change value as low as reasonably achievable or at least below a pre-specified level. A planning study with this technique could be performed for this patient cohort to determine if, through changes in optimization, the probability of image change could be reduced while maintaining the standard-of-care plan quality. Such a study, if successful, would provide strong evidence to support a clinical trial in which traditional planning and optimization were compared to the new method with the goal of reducing normal tissue effects.

In addition, my method is easily generalizable to any other anatomical site for which there is a response that can be identified by imaging. As it stands, my model was used only for MR image changes in the brain, but it could be expanded to other imaging modalities. Advanced

imaging modalities which provide quantitative functional information could potentially greatly improve my model. Being able to tie information on functional anatomical changes back to proton physical properties could pave the way for a new generation of proton biological effects models for a number of different outcomes of interest.

Moreover to improve upon the current results, considerable further research can be performed to improve the accuracy of underlying data used in the analyses and improve the accuracy and robustness of the model and its predictive power. One of the immediate shifts to be made will be to compute the patient treatment plans with a track-repeating algorithm capable of calculating LET_d , as well as variable RWD without the need for such significant post processing⁹¹⁻⁹⁵. This rapid calculation technique would also allow for more laborious calculations for specific cases of interest. One specific example of this type of calculation would be the collection of proton energy or LET spectra on a voxel basis. This data could be used to gain a better understanding of how higher LET components of average LET may play a role in observed biological effects.

To conclude, I have been able to show that proton radiation induced imaging changes in the brain and brainstem are related not only to proton dose but also LET and thus the variable biological effectiveness of protons. The developed model has potential for improving patient treatment plans through its incorporation into plan evaluation and optimization. The voxel-based analysis performed here could be extended to other sites and imaging modalities, which holds promise to further expand the knowledge of in vivo variable proton biological effectiveness.

Bibliography

1. Koehler AM, Schneider RJ, Sisterson JM. Flattening of proton dose distributions for large-field radiotherapy. *Med Phys*. 1977;4(4):297-301. doi:10.1118/1.594317.
2. Koehler AM, Schneider RJ, Sisterson JM. Range modulators for protons and heavy ions. *Nucl Instrum Methods*. 1975;131(3):437-440. doi:10.1016/0029-554X(75)90430-9.
3. Kanai T, Kawachi K, Kumamoto Y, Ogawa H, Yamada T, Matsuzawa H, Inada T. Spot scanning system for proton radiotherapy. *Med Phys*. 1980;7(4):365-369. doi:10.1118/1.594693.
4. Pedroni E, Bacher R, Blattmann H, Böhringer T, Coray A, Lomax A, Lin S, Munkel G, Scheib S, Schneider U, Tourovsky A. The 200-MeV proton therapy project at the Paul Scherrer Institute: Conceptual design and practical realization. *Med Phys*. 1995;22(1):37-53. doi:10.1118/1.597522.
5. Soukup M, Fippel M, Alber M. A pencil beam algorithm for intensity modulated proton therapy derived from Monte Carlo simulations. *Phys Med Biol*. 2005;50(21):5089-5104. doi:10.1088/0031-9155/50/21/010.
6. Lomax A. Intensity modulation methods for proton radiotherapy. *Phys Med Biol*. 1999;44(1):185.
7. Goitein M, Niemierko A. Intensity modulated therapy and inhomogeneous dose to the tumor: a note of caution. *Int J Radiat Oncol Biol Phys*. 1996;36(2):519-522.
8. Grassberger C, Paganetti H. Elevated LET components in clinical proton beams. *Phys Med Biol*. 2011;56(20):6677-6691. doi:10.1088/0031-9155/56/20/011.
9. Grassberger C, Trofimov A, Lomax A, Paganetti H. Variations in Linear Energy Transfer Within Clinical Proton Therapy Fields and the Potential for Biological Treatment Planning. *Int J Radiat Oncol*. 2011;80(5):1559-1566. doi:10.1016/j.ijrobp.2010.10.027.

10. Belli M, Cera F, Cherubini R, Dalla V, Haqjue AMI, Ianzini F, Moschini G, Sapora O, Simone G, Tabocchini MA, Tiveron P. RBE-LET relationships for cell inactivation and mutation induced by low energy protons in V79 cells: Further results at the LNL facility. *Int J Radiat Biol.* 1998;74(4):501-509. doi:10.1080/095530098141375.
11. Chaudhary P, Marshall TI, Perozziello FM, Manti L, Currell FJ, Hanton F, McMahon SJ, Kavanagh JN, Cirrone GAP, Romano F, Prise KM, Schettino G. Relative Biological Effectiveness Variation Along Monoenergetic and Modulated Bragg Peaks of a 62-MeV Therapeutic Proton Beam: A Preclinical Assessment. *Int J Radiat Oncol.* 2014;90(1):27-35. doi:10.1016/j.ijrobp.2014.05.010.
12. Guan F, Peeler C, Bronk L, Geng C, Taleei R, Randeniya S, Ge S, Mirkovic D, Grosshans D, Mohan R, Titt U. Analysis of the track- and dose-averaged LET and LET spectra in proton therapy using the geant4 Monte Carlo code. *Med Phys.* 2015;42(11):6234-6247. doi:10.1118/1.4932217.
13. Wilkens JJ, Oelfke U. Analytical linear energy transfer calculations for proton therapy. *Med Phys.* 2003;30(5):806. doi:10.1118/1.1567852.
14. Chatterjee A, Holley WR. Biochemical mechanisms and clusters of damage for high-let radiation. *Adv Space Res.* 1992;12(2-3):33-43. doi:10.1016/0273-1177(92)90087-E.
15. Belli M, Cera F, Cherubini R, Haque AMI, Ianzini F, Moschini G, Sapora O, Simone G, Tabocchini MA, Tiveron P. Inactivation and mutation induction in v79 cells by low energy protons: Re-evaluation of the results at the LNL facility. *Int J Radiat Biol.* 1993;63(3):331-337. doi:10.1080/09553009314550441.
16. Wouters BG, Lam GKY, Oelfke U, Gardey K, Durand RE, Skarsgard LD. Measurements of Relative Biological Effectiveness of the 70 MeV Proton Beam at TRIUMF Using

- Chinese Hamster V79 Cells and the High-Precision Cell Sorter Assay. *Radiat Res.* 1996;146(2):159. doi:10.2307/3579588.
17. Skarsgard LD. Radiobiology with heavy charged particles: A historical review. *Phys Med.* 1998;14(SUPPL. 1):1-19.
 18. Paganetti H, Niemierko A, Ancukiewicz M, Gerweck LE, Goitein M, Loeffler JS, Suit HD. Relative biological effectiveness (RBE) values for proton beam therapy. *Int J Radiat Oncol Biol Phys.* 2002;53(2):407–421.
 19. Guan F, Bronk L, Titt U, Lin SH, Mirkovic D, Kerr MD, Zhu XR, Dinh J, Sobieski M, Stephan C, Peeler CR, Taleei R, Mohan R, Grosshans DR. Spatial mapping of the biologic effectiveness of scanned particle beams: towards biologically optimized particle therapy. *Sci Rep.* 2015;5:9850. doi:10.1038/srep09850.
 20. Paganetti H. Relative biological effectiveness (RBE) values for proton beam therapy. Variations as a function of biological endpoint, dose, and linear energy transfer. *Phys Med Biol.* 2014;59(22):R419-R472. doi:10.1088/0031-9155/59/22/R419.
 21. International Commission on Radiation Units and Measurements, International Atomic Energy Agency. *Prescribing, Recording, and Reporting Proton-Beam Therapy.* Oxford: Oxford Univ. Press; 2007.
 22. Wilkens JJ, Oelfke U. A phenomenological model for the relative biological effectiveness in therapeutic proton beams. *Phys Med Biol.* 2004;49(13):2811-2825. doi:10.1088/0031-9155/49/13/004.
 23. Frese MC, Yu VK, Stewart RD, Carlson DJ. A Mechanism-Based Approach to Predict the Relative Biological Effectiveness of Protons and Carbon Ions in Radiation Therapy. *Int J Radiat Oncol.* 2012;83(1):442-450. doi:10.1016/j.ijrobp.2011.06.1983.

24. Carlson DJ, Stewart RD, Semenenko VA, Sandison GA. Combined Use of Monte Carlo DNA Damage Simulations and Deterministic Repair Models to Examine Putative Mechanisms of Cell Killing. *Radiat Res.* 2008;169(4):447-459. doi:10.1667/RR1046.1.
25. Wedenberg M, Lind BK, Hårdemark B. A model for the relative biological effectiveness of protons: The tissue specific parameter α/β of photons is a predictor for the sensitivity to LET changes. *Acta Oncol.* 2013;52(3):580-588. doi:10.3109/0284186X.2012.705892.
26. Chen Y, Ahmad S. Empirical model estimation of relative biological effectiveness for proton beam therapy. *Radiat Prot Dosimetry.* 2012;149(2):116-123. doi:10.1093/rpd/ncr218.
27. Carabe-Fernandez A, Dale RG, Jones B. The incorporation of the concept of minimum RBE (RBE_{min}) into the linear-quadratic model and the potential for improved radiobiological analysis of high-LET treatments. *Int J Radiat Biol.* 2007;83(1):27-39. doi:10.1080/09553000601087176.
28. Carabe-Fernandez A, Dale RG, Hopewell JW, Jones B, Paganetti H. Fractionation effects in particle radiotherapy: implications for hypo-fractionation regimes. *Phys Med Biol.* 2010;55(19):5685-5700. doi:10.1088/0031-9155/55/19/005.
29. Polster L, Schuemann J, Rinaldi I, Burigo L, McNamara AL, Stewart RD, Attili A, Carlson DJ, Sato T, Ramos Méndez J, Faddegon B, Perl J, Paganetti H. Extension of TOPAS for the simulation of proton radiation effects considering molecular and cellular endpoints. *Phys Med Biol.* 2015;60(13):5053-5070. doi:10.1088/0031-9155/60/13/5053.
30. Frese MC, Wilkens JJ, Huber PE, Jensen AD, Oelfke U, Taheri-Kadkhoda Z. Application of Constant vs. Variable Relative Biological Effectiveness in Treatment Planning of Intensity-Modulated Proton Therapy. *Int J Radiat Oncol.* 2011;79(1):80-88. doi:10.1016/j.ijrobp.2009.10.022.

31. Carabe A, Moteabbed M, Depauw N, Schuemann J, Paganetti H. Range uncertainty in proton therapy due to variable biological effectiveness. *Phys Med Biol.* 2012;57(5):1159-1172. doi:10.1088/0031-9155/57/5/1159.
32. McNamara AL, Schuemann J, Paganetti H. A phenomenological relative biological effectiveness (RBE) model for proton therapy based on all published *in vitro* cell survival data. *Phys Med Biol.* 2015;60(21):8399-8416. doi:10.1088/0031-9155/60/21/8399.
33. Stewart RD, Yu VK, Georgakilas AG, Koumenis C, Park JH, Carlson DJ. Effects of Radiation Quality and Oxygen on Clustered DNA Lesions and Cell Death. *Radiat Res.* 2011;176(5):587-602. doi:10.1667/RR2663.1.
34. Goodhead DT, Belli M, Mill AJ, Bance DA, Allens LA, Hall SC, Ianzani F, Simone G, Stevens DL, Stretch A, Tabocchini MA, Wilkinson RE. Direct comparison between protons and alpha-particles of the same LET: I. Irradiation methods and inactivation of asynchronous v79, hela and c3h 10t1/2 cells. *Int J Radiat Biol.* 1992;61(5):611-624. doi:10.1080/09553009214551421.
35. Blomquist E, Russell KR, Stenerl w B, Montelius A, Grusell E, Carlsson J. Relative biological effectiveness of intermediate energy protons. Comparisons with ⁶⁰Co gamma-radiation using two cell lines. *Radiother Oncol.* 1993;28(1):44-51. doi:10.1016/0167-8140(93)90184-A.
36. Folkard M, Prise KM, Vojnovic B, Newman HC, Roper MJ, Michael BD. Inactivation of V79 cells by low-energy protons, deuterons and helium-3 ions. *Int J Radiat Biol.* 1996;69(6):729-738. doi:10.1080/095530096145472.
37. Schettino G, Folkard M, Prise KM, Vojnovic B, Bowey AG, Michael BD. Low-Dose Hypersensitivity in Chinese Hamster V79 Cells Targeted with Counted Protons Using a

- Charged-Particle Microbeam. *Radiat Res.* 2001;156(5):526-534. doi:10.1667/0033-7587(2001)156[0526:LDHICH]2.0.CO;2.
38. Wilkens JJ, Oelfke U. Direct Comparison of Biologically Optimized Spread-out Bragg Peaks for Protons and Carbon Ions. *Int J Radiat Oncol.* 2008;70(1):262-266. doi:10.1016/j.ijrobp.2007.08.029.
39. Coutrakon G, Cortese J, Ghebremedhin A, Hubbard J, Johanning J, Koss P, Maudsley G, Slater CR, Zuccarelli C, Robertson J. Microdosimetry spectra of the Loma Linda proton beam and relative biological effectiveness comparisons. *Med Phys.* 1997;24(9):1499-1506. doi:10.1118/1.598038.
40. Semenenko VA, Stewart RD. A Fast Monte Carlo Algorithm to Simulate the Spectrum of DNA Damages Formed by Ionizing Radiation. *Radiat Res.* 2004;161(4):451-457. doi:10.1667/RR3140.
41. Semenenko VA, Stewart RD, Ackerman EJ. Monte Carlo Simulation of Base and Nucleotide Excision Repair of Clustered DNA Damage Sites. I. Model Properties and Predicted Trends. *Radiat Res.* 2005;164(2):180-193. doi:10.1667/RR3402.
42. Semenenko VA, Stewart RD. Monte Carlo Simulation of Base and Nucleotide Excision Repair of Clustered DNA Damage Sites. II. Comparisons of Model Predictions to Measured Data. *Radiat Res.* 2005;164(2):194-201. doi:10.1667/RR3414.
43. Semenenko VA, Stewart RD. Fast Monte Carlo simulation of DNA damage formed by electrons and light ions. *Phys Med Biol.* 2006;51(7):1693-1706. doi:10.1088/0031-9155/51/7/004.
44. Butts JJ, Katz R. Theory of RBE for Heavy Ion Bombardment of Dry Enzymes and Viruses. *Radiat Res.* 1967;30(4):855-871. doi:10.2307/3572151.

45. Scholz M, Kraft G. Calculation of Heavy Ion Inactivation Probabilities Based on Track Structure, X Ray Sensitivity and Target Size. *Radiat Prot Dosimetry*. 1994;52(1-4):29-33.
46. Scholz M, Kraft G. Track structure and the calculation of biological effects of heavy charged particles. *Adv Space Res*. 1996;18(1-2):5-14.
47. Scholz M, Kellerer AM, Kraft-Weyrather W, Kraft G. Computation of cell survival in heavy ion beams for therapy. *Radiat Environ Biophys*. 1997;36(1):59–66.
48. Lyman JT. Complication Probability as Assessed from Dose-Volume Histograms. *Radiat Res*. 1985;104(2):S13. doi:10.2307/3576626.
49. Kutcher GJ, Burman C. Calculation of complication probability factors for non-uniform normal tissue irradiation: The effective volume method gerald. *Int J Radiat Oncol Biol Phys*. 1989;16(6):1623-1630. doi:10.1016/0360-3016(89)90972-3.
50. Emami B, Lyman J, Brown A, Cola L, Goitein M, Munzenrider JE, Shank B, Solin LJ, Wesson M. Tolerance of normal tissue to therapeutic irradiation. *Int J Radiat Oncol*. 1991;21(1):109-122. doi:10.1016/0360-3016(91)90171-Y.
51. Burman C, Kutcher GJ, Emami B, Goitein M. Fitting of normal tissue tolerance data to an analytic function. *Int J Radiat Oncol*. 1991;21(1):123-135. doi:10.1016/0360-3016(91)90172-Z.
52. Ellenberg L, McComb GJMD, Siegel SEMD, Stowe SMD. Factors Affecting Intellectual Outcome in Pediatric Brain Tumor Patients. *Neurosurgery*. 1987;21(5):638-644.
53. Copeland DR, deMoor C, Iii BDM, Ater JL. Neurocognitive Development of Children After a Cerebellar Tumor in Infancy: A Longitudinal Study. *J Clin Oncol*. 1999;17(11):3476-3486.
54. Kirsch DG, Tarbell NJ. Conformal radiation therapy for childhood CNS tumors. *Oncologist*. 2004;9(4):442-450. doi:10.1634/theoncologist.9-4-442.

55. Kirsch DG, Tarbell NJ. New Technologies in Radiation Therapy for Pediatric Brain Tumors: The Rationale for Proton Radiation Therapy. *Pediatr Blood Cancer*. 2004;42(5):461-464. doi:10.1002/pbc.10471.
56. St. Clair WH, Adams JA, Bues M, Fullerton BC, La Shell S, H.M. Kooy, Loeffler JS, Tarbell NJ. Advantage of protons compared to conventional X-ray or IMRT in the treatment of a pediatric patient with medulloblastoma. *Int J Radiat Oncol Biol Phys*. 2004;58(3):727-734. doi:10.1016/S0360-3016(03)01574-8.
57. Hardy P, Bridge P. What are the potential benefits and limitations of particle therapy in the treatment of paediatric malignancies? *J Radiother Pract*. 2008;7(1):9-18. doi:10.1017/S1460396907006218.
58. Gunther JR, Sato M, Chintagumpala M, Ketonen L, Jones JY, Allen PK, Paulino AC, Okcu MF, Su JM, Weinberg J, Boehling NS, Khatua S, Adesina A, Dauser R, Whitehead WE, Mahajan A. Imaging Changes in Pediatric Intracranial Ependymoma Patients Treated With Proton Beam Radiation Therapy Compared to Intensity Modulated Radiation Therapy. *Int J Radiat Oncol*. 2015;93(1):54-63. doi:10.1016/j.ijrobp.2015.05.018.
59. Waters L, Hendricks J, McKinney G. *MCNPX Version 2.5.0.*; 2005.
60. Russell KR, Grusell E, Montelius A. Dose calculations in proton beams: range straggling corrections and energy scaling. *Phys Med Biol*. 1995;40(6):1031. doi:10.1088/0031-9155/40/6/005.
61. Pflugfelder D, Wilkens JJ, Szymanowski H, Oelfke U. Quantifying lateral tissue heterogeneities in hadron therapy. *Med Phys*. 2007;34(4):1506-1513. doi:10.1118/1.2710329.

62. Paganetti H, Jiang H, Parodi K, Slopesma R, Engelsman M. Clinical implementation of full Monte Carlo dose calculation in proton beam therapy. *Phys Med Biol*. 2008;53(17):4825-4853. doi:10.1088/0031-9155/53/17/023.
63. Jia Y, Beltran C, Indelicato DJ, Flampouri S, Li Z, Merchant TE. Proton therapy dose distribution comparison between Monte Carlo and a treatment planning system for pediatric patients with ependymoma. *Med Phys*. 2012;39(8):4742-4747. doi:10.1118/1.4736413.
64. Urie M, Goitein M, Holley WR, Chen GTY. Degradation of the Bragg peak due to inhomogeneities. *Phys Med Biol*. 1986;31(1):1. doi:10.1088/0031-9155/31/1/001.
65. Titt U, Sell M, Unkelbach J, Bangert M, Mirkovic D, Oelfke U, Mohan R. Degradation of proton depth dose distributions attributable to microstructures in lung-equivalent material. *Med Phys*. 2015;42(11):6425-6432. doi:10.1118/1.4932625.
66. Sawakuchi GO, Titt U, Mirkovic D, Mohan R. Density heterogeneities and the influence of multiple Coulomb and nuclear scatterings on the Bragg peak distal edge of proton therapy beams. *Phys Med Biol*. 2008;53(17):4605-4619. doi:10.1088/0031-9155/53/17/010.
67. Li Y, Zhang X, Lii M, Sahoo N, Zhu RX, Gillin M, Mohan R. Incorporating partial shining effects in proton pencil-beam dose calculation. *Phys Med Biol*. 2008;53(3):605. doi:10.1088/0031-9155/53/3/007.
68. Liu Q, Ghosh P, Magpayo N, Testa M, Tang S, Gheorghiu L, Biggs P, Paganetti H, Efsthathiou JA, Lu H-M, Held KD, Willers H. Lung Cancer Cell Line Screen Links Fanconi Anemia/BRCA Pathway Defects to Increased Relative Biological Effectiveness of Proton Radiation. *Int J Radiat Oncol*. 2015;91(5):1081-1089. doi:10.1016/j.ijrobp.2014.12.046.
69. Bentzen SM, Constine LS, Deasy JO, Eisbruch A, Jackson A, Marks LB, Ten Haken RK, Yorke ED. Quantitative Analyses of Normal Tissue Effects in the Clinic (QUANTEC): An

Introduction to the Scientific Issues. *Int J Radiat Oncol*. 2010;76(3):S3-S9.

doi:10.1016/j.ijrobp.2009.09.040.

70. Lawrence YR, Li XA, el Naqa I, Hahn CA, Marks LB, Merchant TE, Dicker AP. Radiation Dose–Volume Effects in the Brain. *Int J Radiat Oncol*. 2010;76(3):S20-S27. doi:10.1016/j.ijrobp.2009.02.091.
71. Mayo C, Yorke E, Merchant TE. Radiation Associated Brainstem Injury. *Int J Radiat Oncol • Biol • Phys*. 2010;76(3):S36-S41. doi:10.1016/j.ijrobp.2009.08.078.
72. Elnahal SM, Kerstiens J, Helsper RS, Zietman AL, Johnstone PAS. Proton Beam Therapy and Accountable Care: The Challenges Ahead. *Int J Radiat Oncol*. 2013;85(4):e165-e172. doi:10.1016/j.ijrobp.2012.10.038.
73. Kerstiens J, Johnstone PAS. Proton Therapy Expansion Under Current United States Reimbursement Models. *Int J Radiat Oncol*. 2014;89(2):235-240. doi:10.1016/j.ijrobp.2014.02.014.
74. Verma V, Mishra MV, Mehta MP. A systematic review of the cost and cost-effectiveness studies of proton radiotherapy. *Cancer*. 2016;122(10):1483-1501. doi:10.1002/cncr.29882.
75. Sabin ND, Merchant TE, Harreld JH, Patay Z, Klimo P, Qaddoumi I, Armstrong GT, Wright K, Gray J, Indelicato DJ, Gajjar A. Imaging Changes in Very Young Children with Brain Tumors Treated with Proton Therapy and Chemotherapy. *Am J Neuroradiol*. 2013;34(2):446-450. doi:10.3174/ajnr.A3219.
76. Fouladi M, Chintagumpala M, Laningham FH, Ashley D, Kellie SJ, Langston JW, McCluggage CW, Woo S, Kocak M, Krull K, Kun LE, Mulhern RK, Gajjar A. White Matter Lesions Detected by Magnetic Resonance Imaging After Radiotherapy and High-Dose Chemotherapy in Children With Medulloblastoma or Primitive Neuroectodermal Tumor. *J Clin Oncol*. 2004;22(22):4551-4560. doi:10.1200/JCO.2004.03.058.

77. Helton KJ, Edwards M, Steen RG, Merchant TE, Sapp MV, Boop FA, Langston J. Neuroimaging-detected late transient treatment-induced lesions in pediatric patients with brain tumors. *J Neurosurg*. 2005;102(2):179-186. doi:10.3171/jns.2005.102.2.0179.
78. National Cancer Institute. *Common Terminology Criteria for Adverse Events v4.0*. NIH publication # 09-7473. NCI, NIH, DHHS; 2009.
79. Cheung M, Chan AS, Law SC, Chan JH, Tse VK. COgnitive function of patients with nasopharyngeal carcinoma with and without temporal lobe radionecrosis. *Arch Neurol*. 2000;57(9):1347-1352. doi:10.1001/archneur.57.9.1347.
80. Zhou X, Ou X, Xu T, Wang X, Shen C, Ding J, Hu C. Effect of Dosimetric Factors on Occurrence and Volume of Temporal Lobe Necrosis Following Intensity Modulated Radiation Therapy for Nasopharyngeal Carcinoma: A Case-Control Study. *Int J Radiat Oncol*. 2014;90(2):261-269. doi:10.1016/j.ijrobp.2014.05.036.
81. Jeraj R, Cao Y, Ten Haken RK, Hahn C, Marks L. Imaging for Assessment of Radiation-Induced Normal Tissue Effects. *Int J Radiat Oncol*. 2010;76(3):S140-S144. doi:10.1016/j.ijrobp.2009.08.077.
82. Giantsoudi D, Sethi RV, Yeap BY, Eaton BR, Ebb DH, Caruso PA, Rapalino O, Chen Y-LE, Adams JA, Yock TI, Tarbell NJ, Paganetti H, MacDonald SM. Incidence of CNS Injury for a Cohort of 111 Patients Treated With Proton Therapy for Medulloblastoma: LET and RBE Associations for Areas of Injury. *Int J Radiat Oncol*. 2016;95(1):287-296. doi:10.1016/j.ijrobp.2015.09.015.
83. Sethi RV, Giantsoudi D, Raiford M, Malhi I, Niemierko A, Rapalino O, Caruso P, Yock TI, Tarbell NJ, Paganetti H, MacDonald SM. Patterns of Failure After Proton Therapy in Medulloblastoma; Linear Energy Transfer Distributions and Relative Biological

Effectiveness Associations for Relapses. *Int J Radiat Oncol*. 2014;88(3):655-663.

doi:10.1016/j.ijrobp.2013.11.239.

84. Pehlivan B, Ares C, Lomax AJ, Stadelmann O, Goitein G, Timmermann B, Schneider RA, Hug EB. Temporal Lobe Toxicity Analysis After Proton Radiation Therapy for Skull Base Tumors. *Int J Radiat Oncol*. 2012;83(5):1432-1440. doi:10.1016/j.ijrobp.2011.10.042.
85. Zeng L, Huang S-M, Tian Y-M, Sun X-M, Han F, Lu T-X, Deng X-W. Normal Tissue Complication Probability Model for Radiation-induced Temporal Lobe Injury after Intensity-modulated Radiation Therapy for Nasopharyngeal Carcinoma. *Radiology*. 2015;276(1):243-249. doi:10.1148/radiol.14141721.
86. van der Maazen RWM, Verhagen I, Kleiboer BJ, van der Kogel AJ. Radio sensitivity of glial progenitor cells of the perinatal and adult rat optic nerve studied by an in vitro clonogenic assay. *Radiother Oncol*. 1991;20(4):258-264. doi:10.1016/0167-8140(91)90125-Z.
87. van der Maazen RWM, Kleiboer BJ, Verhagen I, van der Kogel AJ. Repair capacity of adult rat glial progenitor cells determined by an in vitro clonogenic assay after in vitro or in vivo fractionated irradiation. *Int J Radiat Biol*. 1993;63(5):661-666. doi:10.1080/09553009314450861.
88. Calvo W, Hopewell JW, Reinhold HS, Yeung TK. Time- and dose-related changes in the white matter of the rat brain after single doses of X rays. *Br J Radiol*. 1988;61(731):1043-1052.
89. Reinhold HS, Calvo W, Hopewell JW, Van DB. Development of blood vessel-related radiation damage in the fimbria of the central nervous system. *Int J Radiat Oncol Biol Phys*. 1990;18(1):37-42. doi:10.1016/0360-3016(90)90264-K.

90. Lyubimova N, Hopewell JW. Experimental evidence to support the hypothesis that damage to vascular endothelium plays the primary role in the development of late radiation-induced CNS injury. *Br J Radiol.* 2004;77(918):488-492.
doi:10.1259/bjr/15169876.
91. Yepes P, Randeniya S, Taddei PJ, Newhauser WD. A track-repeating algorithm for fast Monte Carlo dose calculations of proton radiotherapy. *Nucl Technol.* 2009;168(3):736-740.
92. Yepes PP, Eley JG, Liu A, Mirkovic D, Randeniya S, Titt U, Mohan R. Validation of a track repeating algorithm for intensity modulated proton therapy: Clinical cases study. *Phys Med Biol.* 2016;61(7):2633-2645. doi:10.1088/0031-9155/61/7/2633.
93. Yepes PP, Brannan T, Huang J, Mirkovic D, Newhauser WD, Taddei PJ, Titt U. Application of a fast proton dose calculation algorithm to a thorax geometry. *Radiat Meas.* 2010;45(10):1367-1368. doi:10.1016/j.radmeas.2010.05.022.
94. Yepes P, Randeniya S, Taddei PJ, Newhauser WD. Monte Carlo fast dose calculator for proton radiotherapy: Application to a voxelized geometry representing a patient with prostate cancer. *Phys Med Biol.* 2009;54(1):N21-N28. doi:10.1088/0031-9155/54/1/N03.
95. Yepes PP, Mirkovic D, Taddei PJ. A GPU implementation of a track-repeating algorithm for proton radiotherapy dose calculations. *Phys Med Biol.* 2010;55(23):7107-7120.
doi:10.1088/0031-9155/55/23/S11.

Vita

Christopher Ryan Peeler was born in Houma, Louisiana on September 11, 1988, the son of Carla Marie Peeler and Charles Ronald Peeler. After completing his work at Vandebilt Catholic High School, Houma, Louisiana in 2006, he entered Louisiana State University in Baton Rouge, Louisiana. He received the degree of Bachelor of Science with a major in physics from LSU in May, 2010. In September of 2010 he entered The University of Texas Graduate School of Biomedical Sciences at Houston.

Permanent address:

3660 Richmond Ave., Apt. 327

Houston, Texas 77046